

## Contents

<b>1</b>	<b>Executive Summary</b>	<b>1</b>
<b>2</b>	<b>Relevance to NASA Objectives</b>	<b>2</b>
<b>3</b>	<b>Scientific Program</b>	<b>3</b>
3.1	Background . . . . .	3
3.1.1	History of Star Formation . . . . .	3
3.1.2	Astrophysics of [CII] . . . . .	4
3.2	Science Goals . . . . .	5
3.2.1	A Star Formation Evolution Survey Using [CII] (Science Goal 1) . . . . .	6
3.2.2	Power Spectrum of [CII](Science Goal 2) . . . . .	6
<b>4</b>	<b>Instrument</b>	<b>8</b>
4.1	Design Considerations and Sensitivity . . . . .	8
4.2	Spectrometer Architecture . . . . .	10
4.3	Kinetic-Inductance Detector (KID) Arrays . . . . .	10
4.4	Readouts . . . . .	14
4.5	Telescope . . . . .	15
4.6	Cryogenics . . . . .	15
4.7	Pointing and System . . . . .	16
<b>5</b>	<b>Flight Operations</b>	<b>17</b>
5.1	Scheduling . . . . .	17
5.2	In-Flight Data Operations . . . . .	18
<b>6</b>	<b>Plan of Work</b>	<b>18</b>
6.1	Schedule . . . . .	18
6.2	Division of Labor and Personnel . . . . .	19

*Note: As per the ROSES-2011 Solicitation NNH11ZDA001N Appendix D.3 Section 1.2.2.3: Owing to the anticipated greater degree of complexity, the scientific/technical/ management section of proposals for a suborbital flight investigation may be 20 pages long instead of the default 15 pages specified in the NASA Guidebook for Proposers.*

## 1. EXECUTIVE SUMMARY

Understanding the formation and evolution of galaxies is one of the foremost goals of astrophysics and cosmology today. The cosmic star formation rate has undergone a dramatic evolution of the course of the last seven billion years. Dust-obscured star forming galaxies (DSFGs) offer the perfect tracers of this evolution as they contain much of the star-forming activity. By their very nature, DSFGs are difficult to study and have, until recently, been poorly understood. A variety of unextincted diagnostic lines are present in the far-infrared (FIR) which can provide insight into the conditions of star formation, including the instantaneous star formation rate, the effect of AGN feedback on star formation, the mass function of the stars, and the spectrum of their ionizing radiation.

Spectroscopy in the far-infrared is technically difficult but scientifically crucial, as underscored by the Decadal Review's endorsement of US involvement in the Japanese-led Space Infrared Telescope for Cosmology and Astrophysics (SPICA), a 4 K, 3 meter telescope optimized for FIR spectroscopy. Involvement at the level of a complete NASA-funded instrument now seems unlikely in the current budgetary environment (though small critical hardware contributions are under consideration). FIR spectroscopy from space-based platform with a cryogenic mirror can, in principle, achieve performance limited by astrophysical backgrounds. However, we argue that stratospheric balloons offer a platform which can outperform current capabilities and are competitive against satellite missions for large area, spatial/spectral mapping. This is possible for a telescope using low-emissivity, high-throughput optics onto a dispersive spectrometer, and having high-sensitivity, large-format detector arrays.

We propose an aggressive program of instrumentation development and experimental study called the Spectroscopic Terahertz Airborne Receiver for Far-InfraRed Exploration (STARFIRE), with the goal of demonstrating the key technical milestones necessary for balloon-borne FIR spectroscopy limited by the photon noise from the atmosphere. STARFIRE will address the two key technical issues necessary to achieve this:

1. Low emissivity, high throughput telescope and spectrometer optics
2. Background limited detectors in large format arrays, scalable to  $> 10^4$  pixels

We will do this by constructing an integral-field spectrometer from 240 - 420  $\mu\text{m}$  coupled to a 2.5 m off-axis telescope. For the detectors, we will leverage the highly advanced development work of Jonas Zmuidzinas' group at Caltech / JPL on kinetic inductance detectors (KIDs). KIDs represent the most promising route to economical, large format submillimeter detector arrays. In addition to this technical demonstration, we will be able to obtain scientific results from STARFIRE from two North American overnight flights which will

1. Obtain spectra of  $\sim 100$  galaxies in the fine structure lines [CII](157  $\mu\text{m}$ ) ( $0.5 < z < 1.54$ ), and for lensed galaxies, [OI](63  $\mu\text{m}$ ), and [OIII](88  $\mu\text{m}$ ) ( $2 < z < 4$ )
2. Demonstrate deep tomographic maps capable of detecting the shot noise power spectrum of [CII] at  $z \sim 1$

With these goals met, it is our explicit intention to build upon this proposal in order to successfully propose a wholly unprecedented experiment to study the cosmic star formation history. This future experiment will make a 3-D cube spanning spanning at once at least 4 billion years of cosmic history ( $0.5 < z < 1.5$ ), on scales from 1 - 50 Mpc ( $30''$  to  $> 1^\circ$ ) with complete spectroscopic information. This would be done with fully three dimensional tomographic maps of emission in [CII] and other lines. Such an experiment fills a unique and vital scientific niche not filled by *Herschel*, SOFIA, ALMA, or even SPICA.

We stress that much of the work for STARFIRE, including the telescope and spectrometer optics, detectors, and detector readout, can be directly re-used in a future experiment. The frequency domain RF readout of KIDs is relatively inexpensive per pixel, and highly scalable, and the detectors themselves can be swapped out while maintaining the same readout. We note there is still significant discovery potential with STARFIRE, since it will be probing an under-explored wavelength range with unprecedented sensitivity.

## 2. RELEVANCE TO NASA OBJECTIVES

STARFIRE advances NASA's strategic scientific and technical goals in a wide variety of ways. Broadly, STARFIRE supports Goal 2 of the NASA 2011 Strategic Plan to "Expand scientific understanding of the Earth and the universe which we live", specifically addressing sub-goal 2.4 to "discover how the universe works and explore how it began and evolved". The proposal is relevant to NASA's 2007 Science Plan in addressing the Science Question: "How do planets, stars, galaxies, and cosmic structure come into being?"

- STARFIRE takes the next leap in our understanding of the universe by moving from far-IR imaging to far-IR spectroscopy with an order of magnitude improvement in current capabilities. *Herschel* will soon be exhausted of cryogens, and ALMA Band 9 (420 – 500  $\mu\text{m}$ ) is just coming online. STARFIRE will cover the spectral range 240  $\mu\text{m}$ - 420  $\mu\text{m}$ , bridging the gap between *Herschel*-PACS and ALMA Band 9, a wavelength range nearly completely inaccessible from the ground<sup>1</sup>. STARFIRE will have sensitivity to extragalactic spectra more than an order of magnitude greater than the *Herschel*-SPIRE FTS (in their region of spectral overlap), and will be significantly more sensitive than any instrument on SOFIA for extragalactic sources; see Figure 1. STARFIRE observations will provide new data not available from existing facilities to complement the X-ray to radio data from satellites (*Chandra*, *XMM*, *HST*, *Spitzer*, *Herschel*, *Planck*, *AKARI*), airborne (SOFIA) and ground-based telescopes (Gemini, Subaru, VLT, UKIRT, VISTA, Keck) participating in the NASA ORIGINS program.
- STARFIRE addresses the objectives of the APRA solicitation by developing a significant new suborbital platform for submillimeter astronomy, and by dramatically advancing the state-of-the-art in detectors for submillimeter wavelengths. STARFIRE will have the largest number (6000) of the most sensitive far-infrared detectors ever fielded in a scientific instrument. This technical development supports Goal 3 of the NASA 2011 Strategic Plan to "Create the innovative new space technologies for exploration, science, and economic future". Specifically, the STARFIRE program will "develop and demonstrate the critical technologies that will make NASA's exploration, science, and discovery missions more affordable and more capable" (Sub-goal 3.3). This applies to future suborbital missions. Our team has developed and is maintaining significant infrastructure of attitude determination and control that is being exploited by a variety of balloon payloads including EBEX, SPIDER, InFOC $\mu$ S, and HEFT. The STARFIRE telescope is designed with a wide field of view and a generic placement for the receiver, making it very flexible and re-usable, allowing us to easily place upgrades to the STARFIRE spectrometer or new prototype submillimeter receivers there.
- STARFIRE will train the next generation of astrophysicists, from undergraduate and graduate students to postdoctoral fellows. This supports Goal 6 of the NASA 2011 Strategic Plan to "Share NASA with the public, educators, and students to provide opportunities to participate in our Mission, foster innovation, and contribute to a strong national economy". Our previous suborbital sub-millimeter astronomy experiment BLAST produced eight Ph.D.'s and trained several postdocs. It also led to a public documentary film *BLAST!*<sup>2</sup> which supported subgoal 6.4 of the NASA Strategic Plan to "Inform, engage, and inspire the public by sharing NASA's missions, challenges, and results". BLAST also involved over a dozen undergraduates who built hardware, designed parts, and participated in the analysis. For graduate students, suborbital program is the perfect place to learn how to do astrophysics end-to-end, from experimental design to instrument construction to data analysis to theoretical interpretation. STARFIRE will lead to similar achievements on the educational front over the next 5 years, specifically addressing (subgoal 6.1) to "improve retention of students in STEM disciplines by providing opportunities and activities along the full length of the education pipeline."

<sup>1</sup>Note that ALMA Band 10 (787 - 950 GHz; 320 - 380  $\mu\text{m}$ ) will have overlap with STARFIRE, but this will be one of the last bands completed and the most sensitive to weather.

<sup>2</sup><http://www.devlinpix.com/film/blast>

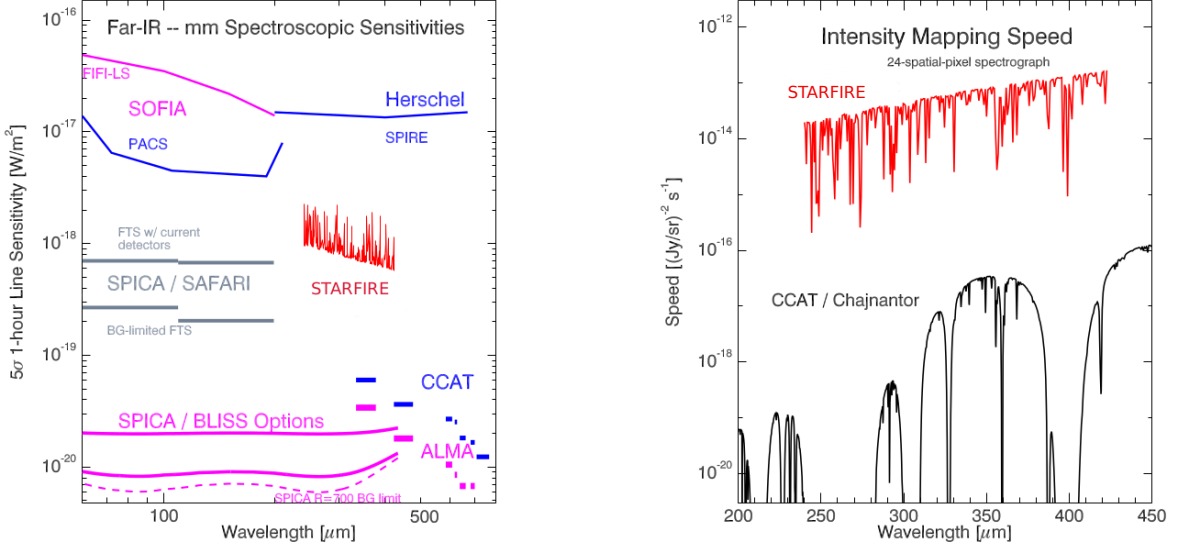


Figure 1: *Left:* STARFIRE (red) compared to current and future spectroscopic instruments. We compute a  $5\sigma$  1 hour sensitivity on a single source as the benchmark. The variation in the STARFIRE sensitivity is due to atmospheric emission lines. Approximately 10% of the band is compromised due to these lines, though they may still be used for frequency calibration. *Right:* The mapping speed of STARFIRE compared to an identical instrument on CCAT. Here larger values correspond to more area mapped to the same depth in the same time; a balloon instrument like STARFIRE is as much as 3 orders of magnitude faster. Note that for intensity mapping, telescope area is not a factor. Note also the significant regions in redshift not accessible from the ground even at the best sites.

### 3. SCIENTIFIC PROGRAM

#### 3.1. Background

##### 3.1.1. History of Star Formation

The detailed story of the formation of galaxies within a cosmological framework is a major unsolved problem in contemporary cosmology (see, e.g., the recent review by 1). Between the end of reionization and about 8 Gyr after the Bang, the cosmic star formation rate density rises steadily, reaching a peak at  $z \sim 2.5$ ; see Figure 2. The nature of the star-forming systems changes dramatically over this period, with the most luminous galaxies at the peak becoming heavily dust enshrouded. Indeed, the discovery of the cosmic far-infrared background (CFIRB) by NASA’s *COBE* satellite (2; 3) and the detection of a significant population of high redshift, dust-obscured galaxies selected at submillimeter (submm) wavelengths (4; 5) revealed that as much as half of the star formation activity in the early Universe occurs in galaxies that are undetected at optical wavelengths (6; 7).

These (sub)millimeter-selected galaxies (hereafter SMGs) which comprise the CFIRB are a cosmologically significant population undergoing intense star formation (with star formation rates of up to  $\sim 10^3 M_\odot \text{ yr}^{-1}$ ) when the Universe was 15 - 45% of its present age, between 7.5 and 11.5 billion years ago. Optical and ultraviolet (UV) radiation from both star formation and AGN activity heat the dust in these galaxies, and this energy is thermally re-radiated at far-infrared (far-IR) to mm wavelengths, with the peak of dust emission occurring at  $\sim 60 - 200 \mu\text{m}$  in the rest-frame (10). The large amount of dust present in them often precludes detailed study at optical wavelengths.

Most studies suggest that the far-IR populations have had a different energy release history from the optically-selected populations, which appear to have experienced a more constant rate of energy release with cosmic time (e.g. (author?) (11)). Further, even for the subset of dusty galaxies for which optical counterparts can be identified and optical spectra obtained, the high obscuration ensures that the optical spectra do not probe the bulk activity in these galaxies. (author?) (12) and others

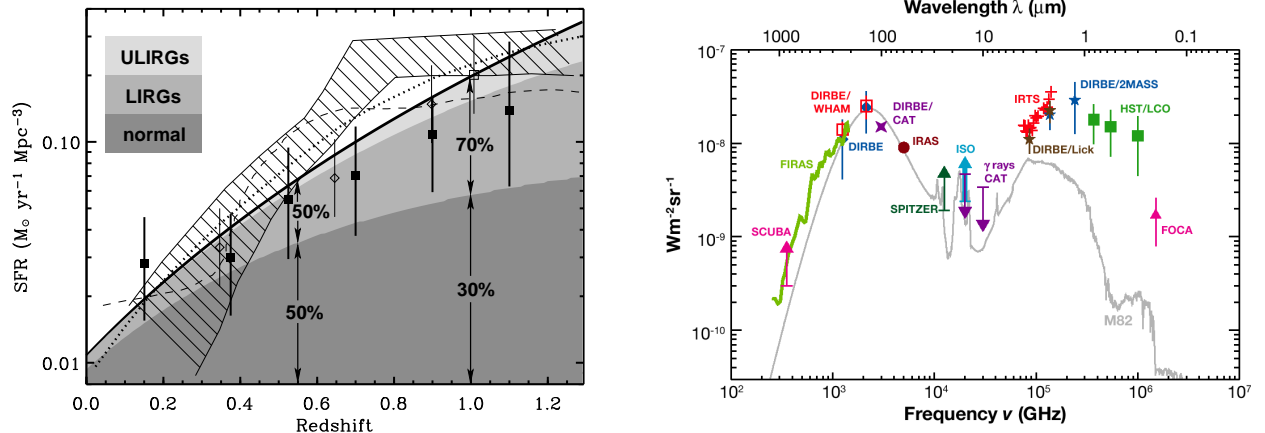


Figure 2: *Left:* The evolution cosmic star formation rate density, broken down by the contributing population, from (author?) (8). *Right:* The fraction of extra-galactic background light due to far-infrared sources (9). Note that roughly equal amounts come from the optical/near-IR and far-IR. Of the far-IR, about half the intensity lies at  $z < 1$ .

have demonstrated this, showing that luminosities based on UV/blue fluxes and colors underestimate the total luminosities of a sample of LIRGs and ULIRGs by factors of 3–75, and that the UV/optical light often comes from regions hundreds of parsecs from the true luminosity sources.

SMGs are thought to mark the formation of the massive elliptical galaxies seen in the local universe (13). The molecular gas masses implied by  $^{12}\text{CO}$  measurements of typical SMGs are  $\sim 10^{10-11} M_\odot$ ; given their inferred star formation rates, this implies that SMGs could have built up all of the stellar mass in spiral bulges or massive elliptical galaxies in a burst of  $10^8$  years duration (14; 15). SMGs have been shown to reside in the most massive dark matter halos at  $z \sim 2.5$  (16; 17). Clustering has been measured for *Herschel* sources, with a distinction detectable between the contributions to clustering from one- and two-halo terms in the models (18).

This population has evolved strongly over the last half of the Universe’s life. The Spitzer 24  $\mu\text{m}$ -selected sources confirm a dramatic decrease in far-infrared luminosity from  $z \sim 1$  to the present: (author?) (19) infer a shift in characteristic luminosity  $L^*$  at a rate of  $(1+z)^{4.0 \pm 0.5}$ . Recent results from BLAST (20) and *Herschel* (?) confirm that about half of the CFIRB was created at  $z < 1$ .

### 3.1.2. Astrophysics of [CII]

The ultraviolet radiation from newly-formed high-mass stars within molecular clouds strongly affects the natal molecular interstellar medium (ISM). Within the immediate stellar vicinity, hydrogen is fully ionized, forming an HII region whose size is set by cloud density and the number of H ionizing (Lyman continuum) photons that are available. Just beyond the HII region, far-UV ( $6 \text{ eV} < h\nu < 13.6 \text{ eV}$ ) photons penetrate the neutral gas where they photoionize atoms and photo-dissociate molecules with ionization or dissociation potentials less than 13.6 eV, forming photodissociation regions (PDRs). The far-UV field strength  $G$  is parametrized in units of the local far-UV radiation field,  $G_0 = 1.6 \times 10^{-3} \text{ erg s}^{-1} \text{ cm}^{-2}$ .

PDRs are an important ISM component: typically 10% by mass in normal Milky-Way-like galaxies, but up to 50% in starbursting nuclei of LIRG and ULIRG galaxies that produce the infrared background. The heating of gas in PDRs is primarily through the photo-electric ejection of energetic electrons from grains, with typical efficiency  $\sim 1\%$ . After gas excitation and dissociation, most of the remaining stellar energy goes into heating dust grains, which re-emit the energy in the far-IR continuum (e.g. (21)). Thus, on small scales where the emitting region is resolved, the far-IR intensity should equal the inferred UV intensity  $G$ . For unresolved galaxies, the ratio of the observed far-IR continuum flux to inferred  $G$  is the beam filling factor, or equivalently the physical size of the starburst region in  $\text{kpc}^2$ .

[CII] is particularly interesting, as it is a primary coolant of these dense PDRs, as well as moderate density “atomic clouds”. It is very luminous, typically the brightest gas-phase feature emitted by galaxies, with up to 1% of the total far-IR luminosity. The measurement of [CII] intensities alone provides important insights into star formation. The [CII]/far-IR continuum luminosity ratio,  $f$ , measures the strength and spatial extent of the starburst.  $f$  is strongly inversely proportional to UV field strength  $G$  for  $G \sim 10^1$  to  $10^4$ , maximizing at 1% for  $G \sim 10$  and  $n \sim 10^3 \text{ cm}^{-3}$ . The inverse relation occurs because the efficiency of photoelectric heating is reduced at high  $G$  due to the build-up of grain charge, and because of the increased gas cooling via the [OI] 63  $\mu\text{m}$  line. Therefore, within these ranges for  $G$  and  $n$ , the measurement of  $f$  determines  $G$ .

(author?) (22) recently obtained new measurements of [CII] in 13 sources with  $1 < z < 2$  (including a previous detection in (author?) (23)). These starburst dominated systems have  $f \sim 3.1 \times 10^{-3}$  while the AGN dominated systems have  $f \sim 3.3 \times 10^{-4}$ . Thus  $f$  appears to pick out star formation dominated systems. This survey also showed that, unlike local starbursts and ULIRGS, where starbursts are confined to 100’s of pc scales, starbursts at  $1 < z < 2$  extend over few kpc scales. They also have FUV fields like those found in M82 ( $G \sim 1000$ ) – not the super intense fields found in local ULIRGs ( $G > 10^4$ ). This is important as it suggests that local ULIRGs are a poor model for the super starbursts at  $1 < z < 2$  and expectations about  $f$  based on local systems (e.g. 24; 25) should be informed by more data.

Obtaining [CII] fluxes and continuum measurements permits the measurement of the star formation rate and spatial extent of the starburst in the galaxy, measurements which cannot be done optically. For the brightest objects, star formation rates obtained in this way can be calibrated with multi-wavelength data and unconfused submm SEDs. The star formation history constructed in this way is derived from a well-defined class of galaxies, determined by their [CII]/FIR ratios. The FIR luminosity can be determined from other continuum observations, even in the face of confusion (26).

### 3.2. Science Goals

With STARFIRE, we will use [CII] to assess the properties in star forming galaxies around the midpoint in the Universe’s history ( $0.5 < z < 1.5$ ) in two basic ways (described in detail below): 1) We will probe galaxies with known redshifts, both in single-object detections and with spatial / spectral stacks. 2) We will carry out the first blind intensity mapping experiment in which the aggregate fluctuation power due to [CII] in all galaxies is measured in a 3-D power spectrum analysis.

STARFIRE is a wideband imaging spectrometer for the 240-420  $\mu\text{m}$  range, multiplexing in the spectral and both spatial dimensions simultaneously to achieve these science goals. The key instrument parameters required to achieve the science goals are summarized in Table 1. The instrument details are discussed in greater detail in Section 4 and the observing method in Section 5.

Both experiments will be carried out in fields which are well-observed and have significant multiwavelength coverage, including *Herschel* 250  $\mu\text{m}$  and *Spitzer*, as well as optical and submillimeter spectroscopic redshifts. The H-ATLAS fields such as GAMA12 and GAMA15 are equatorial and visible to ALMA, and provide a number lensed submillimeter galaxies at high redshift  $2 < z < 4$  for [OI] and [OIII]. Further north, there are well-studied small deep fields such as the H-ATLAS NGP, GOODS-N, the Lockman Hole, and the Groth Strip which are available for long integrations testing the intensity mapping and stacking analyses.

We expect that the knowledge of the submillimeter galaxy population will evolve rapidly in the first years of the grant as new results from *Herschel*, SPT, and ALMA first science programs become available, including – crucially – redshifts using CO from ALMA. This new information will be incorporated into our target selection so as to yield the maximum scientific return and the largest number of solid detections. This survey will fill a significant gap in the understanding of the submillimeter galaxy population and the evolution of star formation with cosmic time.

### 3.2.1. A Star Formation Evolution Survey Using [CII] (Science Goal 1)

The relation of  $L_{[CII]}$  to  $L_{FIR}$  has been measured in a range of systems; see Figure 3.2.1, which is taken from the recent compilation of (author?) (27). For most normal galaxies the  $L_{[CII]}/L_{FIR}$  ratio is  $\approx 3 \times 10^{-3}$  (with a  $1\sigma$  scatter of only  $\sim 0.3$  dex), and for these systems the  $L_{[CII]}$  traces the SFR with a known proportionality constant. For sources in the local universe with  $L \gtrsim 10^{12}$ ,  $L_{[CII]}/L_{FIR}$  drops by a factor of  $\sim 5 - 10$ , and  $L_{[CII]}$  no longer scales with SFR, but such rare sources account for only a small fraction of the total SFR density. At  $z = 1 - 2$ , the (author?) (22) results show that the threshold for a significant drop in  $L_{[CII]}/L_{FIR}$  increases to  $L \sim 5 \times 10^{12} L_\odot$  (Figure 3.2.1), such that the fraction of the SFR density contributed by sources with weak [CII] appears to remain negligible at all redshifts. With STARFIRE we will detect [CII] from individual objects with  $L = (1.4 - 3.2) \times 10^{12}$  at  $z = 0.5 - 1.5$ , and use stacking to detect the average  $L_{[CII]}$  from sources in lower luminosity bins. A comparison with  $L_{FIR}$  and other SF tracers in these populations will then provide a measurement of the  $L_{[CII]}/L_{FIR}$  ratio of typical galaxies at each redshift. This ratio, combined with an estimate of the mean [CII] intensity extracted from the power spectrum, will then be used to make a [CII]-based measurement of the SFR density.

Earlier (28; 29) and more recent (30) works have calibrated the conversion from  $L_{[CII]}$  to SFR up to  $z = 0.3$ , identifying caveats in blindly using this relation, particularly for low metallicity systems and high luminosity systems that may contain an AGN or compact starburst. By selecting fields with existing metallicity information, in addition to the continuum data, STARFIRE is positioned to further explore the extendability of a [CII]-SFR relation in a range of galactic environments, a necessary work in preparation for utilizing future high-redshift ( $z > 6$ ) ground-based [CII] observations as a means of understanding cosmic star formation history (31).

(author?) (27) showed that the  $L_{[CII]}/L_{FIR}$  ratio is strongly anti-correlated with the  $L_{FIR}/M_{H_2}$  ratio, with a relationship that holds both at low- and high- $z$  (see Figure 3.2.1). Recent studies of molecular gas at high redshift has demonstrated that the  $L_{FIR}/M_{H_2}$  ratio traces the mode of star formation (major merger vs quiescent), with higher  $L_{FIR}/M_{H_2}$  ratios produced in galaxies undergoing extreme starbursts triggered by a major merger. The low  $L_{[CII]}/L_{FIR}$  ratios seen in the highest luminosity sources (such as the local ULIRGs) is therefore understood to result from the merger-induced starburst, such that a measure of the average  $L_{[CII]}/L_{FIR}$  in each redshift bin will provide an estimate of the fraction of total star formation occurring in merger-induced bursts, compared with in more quiescently star-forming systems.

Figure 4 shows the kinds of spectra expected from STARFIRE in just ten minute integrations, for both unlensed galaxies  $0.5 < z < 1.5$ , and lensed galaxies  $z \sim 3$ .

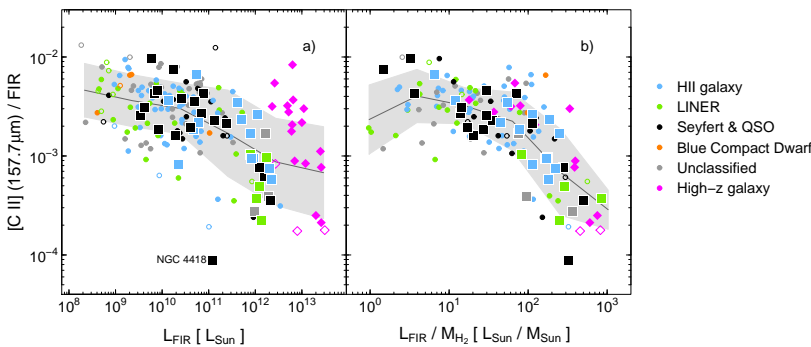


Figure 3: Left: The correlation between [CII] luminosity and FIR luminosity for individual galaxies and the  $L_{FIR}/M_{H_2}$  relation (as compiled in (author?) (27).)

### 3.2.2. Power Spectrum of [CII](Science Goal 2)

Our overarching goal is to connect the process of star formation in individual galaxies via their average properties to the properties of large scale structure (LSS). To do this requires mapping a large cosmic volume, and in addition, traditionally requires large spectroscopic redshift surveys coupled with careful

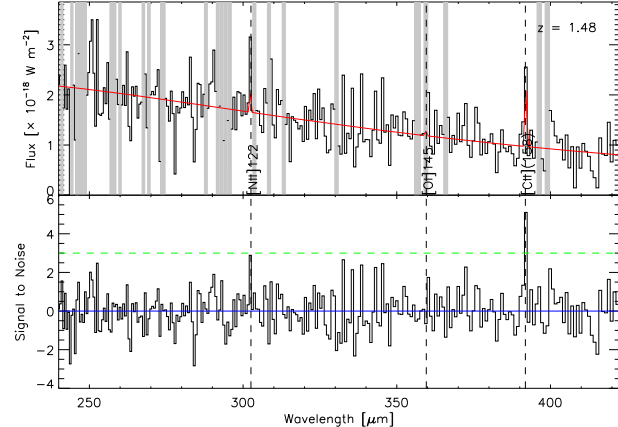
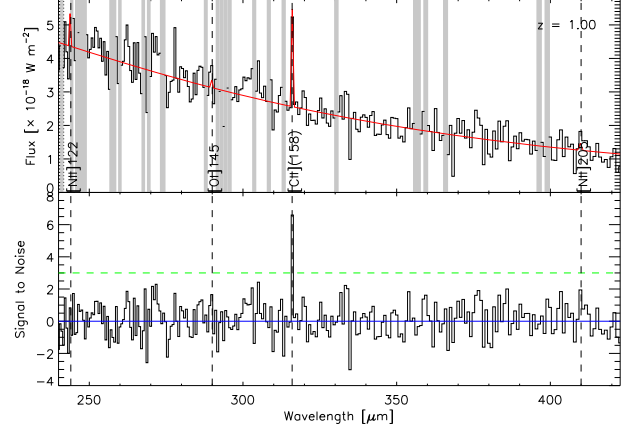
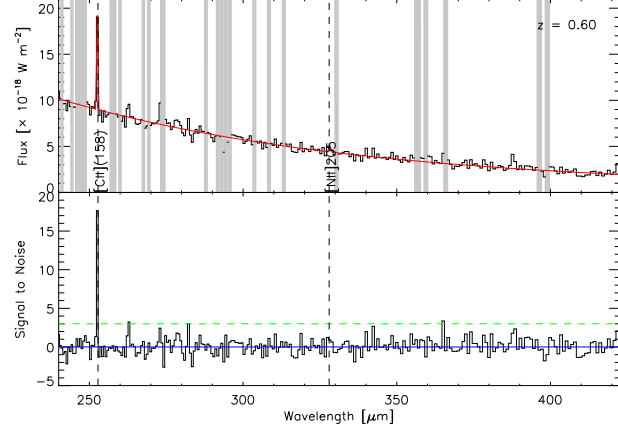


Figure 4: Simulated spectra of galaxies with  $L_{FIR} = 4 \times 10^{12} L_{\odot}$  at various redshifts for which [CII] is accessible to STARFIRE. The observations assumed only 10 minutes of integration time. Note that in addition to the [CII] line, the continuum is strongly detected ( $T_{dust} = 35$  K is assumed), allowing for unambiguous checks on the pointing and calibration. Channels with 2× higher noise than the median are shown in gray (approximately 11% of the total), but the lower panel of each figure shows the signal-to-noise accounting for this increased variance, indicating that these channels, while less sensitive, do not create false positives.

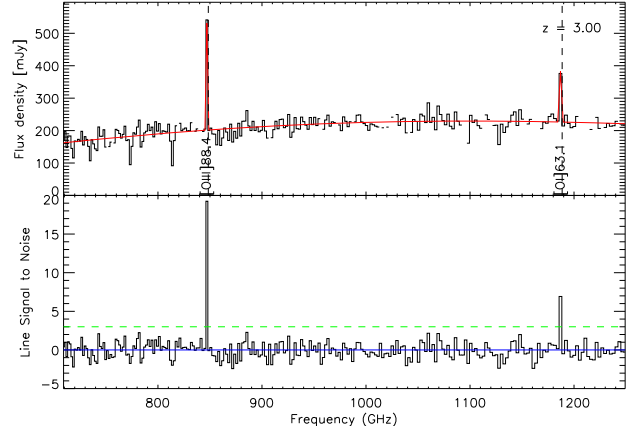
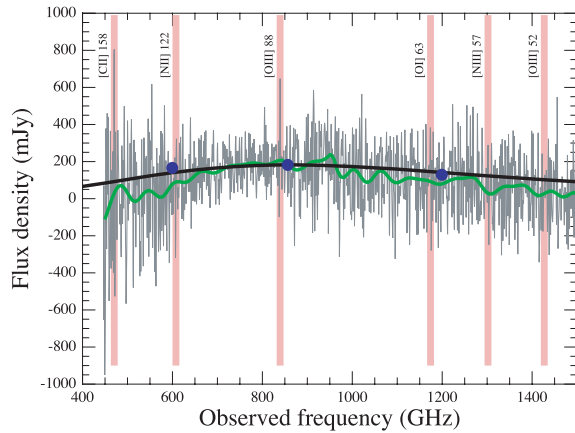


Figure 5: *Left:* The *Herschel*-SPIRE FTS spectrum of SDP.81 from (author?) (32), representing nearly 4 hours of integration time. This galaxy was, at the time of publication, the faintest [CII] line yet detected by *Herschel*. *Right:* A similar galaxy observed for 10 minutes with STARFIRE. Though [CII] has redshifted out of the STARFIRE band, note the clear detection of [OIII](52 μm) as well as [OIII](88 μm).

attention to obtaining photometry for photometric redshifts. However, in the far-IR, the process of obtaining redshifts is difficult and slow. However, the traditional route can be circumvented by *intensity mapping*: making a large data cube in which the third dimension measured a line, thus providing redshift information. In general, individual galaxies are not detected, and the information is extracted from the data via a power spectrum or cross-spectrum.

The most developed case for intensity mapping is that of the 21 cm experiments attempting to detect

the epoch of reionization.<sup>3</sup> At  $z \sim 1$ , intensity mapping using HI has been proposed for measuring baryon acoustic oscillations (BAO 33) and the concept experimentally demonstrated by the detection of the cross-spectrum of HI emission with the DEEP2 galaxy survey (34). Several theoretical studies have recently been published demonstrating the feasibility of doing intensity mapping during the epoch of reionization using CO, [CII] and other transitions in large-beam surveys (35; 36; 37; 31; 38; 39).

With this in mind, we begin by considering the line emission from some particular species  $i$  present in the ISM of galaxies. (We assume any continuum contribution has been removed; this is actually straightforwardly achieved, following schemes which use the spectral smoothness of the continuum to subtract it. See, for example, (author?) (40).) We have an instrument which acts as an integral field spectrometer, mapping an intensity data cube  $S(\alpha, \delta, \nu)$ , where  $(\alpha, \delta)$  are the celestial coordinates of the line-of-sight along which the spectral frequency dimension  $\nu$  is measured. Since we are working with line emission, the observed frequency determines the cosmological redshift and thus  $\nu$  may be transformed into line-of-sight distance, and for each distance, a transverse dimension may also be obtained. Thus  $S(\alpha, \delta, \nu) \Leftrightarrow S(\mathbf{x})$ , where  $\mathbf{x}$  denotes comoving spatial coordinates. The logic of this argument is laid out for the 21 cm HI fluctuations in, for example, (author?) (41). We assume that the extent of  $\mathbf{x}$  in the cube is such that significant cosmological evolution does not occur over the measured region.

Since the galaxies whose line emission we are measuring trace the underlying dark matter potential (with some bias), the intensity field of line emission fluctuations can be written as

$$\Delta S_i(\mathbf{x}) = \bar{S}_i \bar{b} \delta(\mathbf{x}) \quad (1)$$

where  $\bar{S}_i$  is average emission line signal,  $\bar{b}$  is luminosity weighted average galaxy bias, and  $\delta(\mathbf{x})$  is the cosmological overdensity at  $\mathbf{x}$ . In general, since for any realistic instrument the signal-to-noise at any point  $\mathbf{x}$  will be low, we will be concerned with the statistical measures on  $S$ . In particular, the power spectrum of such a signal is

$$P_i(k) = \bar{S}_i^2 (\bar{b}^2 P(k) + P_s) \quad (2)$$

where  $P(k)$  is the matter power spectrum, and we have made the usual assumption of isotropy in the fluctuations.  $P_s$  is a shot (or Poisson) noise term due to the fluctuations of uncorrelated, discrete galaxies, from which we have factored the average line brightness. Note that at the angular scales measured by STARFIRE, the clustering term dominates over the shot noise. Figure 6 shows that a future LDB experiment similar to STARFIRE with 200 hours of integration would be able to measure the power spectrum of [CII] emitters with high signal-to-noise over a range of redshifts and angular scales, accurately measuring the clustering signal. With this proposal, we have the sensitivity to detect the highest- $k$  shot noise and set the scale of the [CII] fluctuations.

## 4. INSTRUMENT

### 4.1. Design Considerations and Sensitivity

To achieve the scientific and technical goals of STARFIRE, we must be able to demonstrate atmosphere-limited performance of the telescope and detectors, and be able to make both pointed observations toward specific objects and small-area maps to validate the sensitivity. The goal is to detect galaxies with  $0.5 < z < 1.5$  in [CII], which sets the wavelength range to 240 - 420  $\mu\text{m}$ .

The design should be such that the sensitivity of the instrument is limited by the photon noise of the atmosphere and optics. To estimate the atmosphere background, the (proprietary) ATM model of Juan Pardo was used. We have assumed a flight at mid-latitudes, an altitude of 37 km, and observations at 45° elevation. The ATM model calculates the opacity due to all relevant atmospheric species. We calculate the noise equivalent power (NEP) due to photon shot noise from a greybody with physical

---

<sup>3</sup>PI Aguirre is currently co-PI of NSF AST 1125558 “Collaborative Research: Precision Array for Probing the Epoch of Reionization (PAPER)”. PAPER is a dedicated attempt to detect the highly redshifted 21 cm emission from the epoch of reionization.

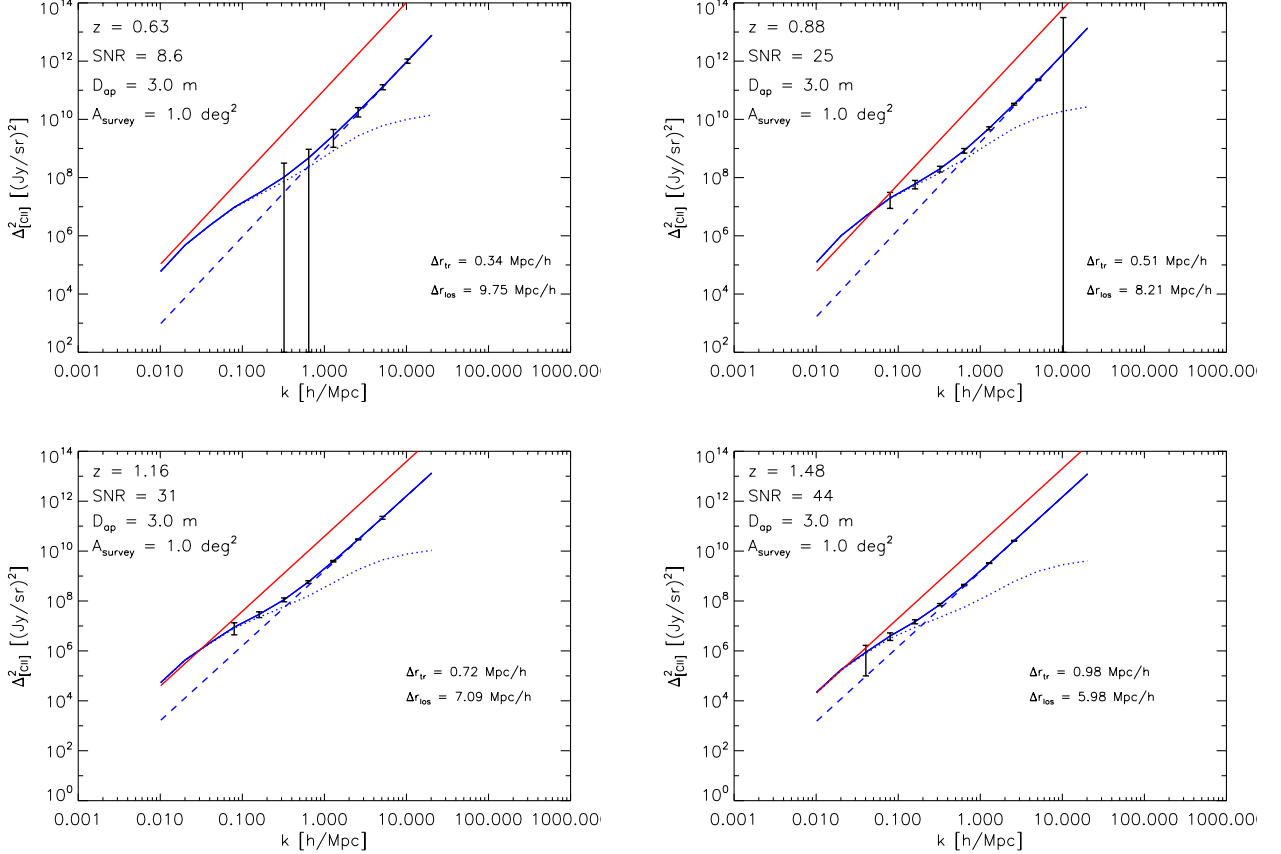


Figure 6: Predicted power spectra for the [CII] line at four redshifts. Dashed lines show the one- and two-halo clustering terms, and the dotted line shows “shot noise” or Poisson term from unclustered galaxies. Note that the clustering raises the amplitude of the power spectrum many orders of magnitude above the shot noise expectation. The vertical black dash-dotted lines indicate the range of scales probed by STARFIRE, i.e., those between  $[(2\pi)^3/V_s]^{1/3}$  and  $[(2\pi)^3/V_{pix}]^{1/3}$ , where  $V_s$  and  $V_{pix}$  are total survey volume and pixel volume respectively.

temperature  $T$  and emissivity  $\epsilon_\nu$  being detected by a system with optical efficiency  $\eta$  as

$$\text{NEP}_\gamma = \sqrt{\frac{N_{pol}}{2}} 2h\nu \sqrt{n(n+1)\Delta\nu} \quad , \quad n = \frac{\eta\epsilon_\nu}{\exp(h\nu/kT) - 1} \quad (3)$$

where  $n$  is the photon occupation number. The detector NEP must be less than the noise  $\text{NEP}_\gamma$ . The low noise detectors we will use for STARFIRE are discussed in Section ???. The final figure of merit for detecting an unresolved line in a point source is given by the line sensitivity

$$\mathcal{S}_\gamma = \frac{2}{N_{pol}} \frac{\sqrt{2}\text{NEP}_\gamma}{\eta_{opt} A_{eff} e^{-\tau_\nu}} \quad \left[ \frac{\text{W}}{\text{m}^2} \sqrt{\text{sec}} \right] \quad (4)$$

where  $\tau_\nu$  is the atmosphere optical depth, related to the emissivity as  $\epsilon_\nu = 1 - \exp(-\tau_\nu)$ . The effective collecting area,  $A_{eff}$ , of the telescope is decreased from the geometrical value  $A = \pi(D_{tel}/2)^2$  by the illumination of the optics.

We have considered the performance of various potential architectures for STARFIRE, incorporating the atmospheric transmission and loading, a range of telescope sizes, and the possibility of actively cooling the telescope to minimize its thermal emission. While a cooled aperture performs better, it is very costly for a given aperture size, and the performance improvement is modest because even a balloon altitudes there is  $\sim 1\%$  emission from the 250 K atmosphere. In light of these

calculations, and our experience with ballooning with BLAST (42; 43) and spectroscopy with Z-Spec (44; 45; 46; 47; 48), we have arrived at a 2.5 m off-axis ambient-temperature telescope, with carefully controlled illumination to avoid spillover to warm surfaces. These parameters and sensitivity factors for our design are given in Table 1.

For optimal sensitivity to line emission in distant galaxies, the spectral resolving power  $R \equiv \lambda/\Delta\lambda$  should be matched to the line width. For the relatively massive galaxies we are targeting, a resolution  $R = 450$  ( $670 \text{ km s}^{-1}$ ) is adequate: higher resolution increases the number of detectors required and may over-resolve the line. In principle, the required spectral resolution and large area mapping could be achieved with either a Fabry-Perot (FP) or FTS spectrometer design. However, both of these require a moving component, and both incur sensitivity penalties. The FP does not cover the entire frequency range instantaneously and must be scanned, and the FTS places the full optical bandwidth of the entire band on each detector, increasing the noise. The best approach is a reflective, blazed diffraction grating, which offers large instantaneous bandwidth and good sensitivity.

## 4.2. Spectrometer Architecture

To achieve integral-field spectroscopy over a 2-D field, the spectrometer optics begin by slicing a  $5 \times 5$  pixel field to form a 25 pixel long pseudo-slit, which feeds the spectrometer. For optimal efficiency, two independent spectrometer modules and image slicers with separate fields of view are combined to cover the full 240-420  $\mu\text{m}$  range: a short wavelength module covering 240-317  $\mu\text{m}$ , and a long wavelength module covering 317-420  $\mu\text{m}$ . The slicing optics follow the same design as successfully implemented in the PACS and FIFI-LS spectrometers (49; 50); see Figure 7.

In Figure 8 we show the long wavelength spectrometer module. A powered mirror collimates the light passing through the pseudo-slit, and forms an image of the telescope aperture on the grating. The grating itself serves as a cold pupil that controls the telescope illumination. The grating is operated in first order, and is sized to provide a slit-limited resolving power of  $R = 450$ . A second powered mirror then focuses the dispersed light onto the focal plane. The long wavelength module has a size of  $60 \times 32 \times 22 \text{ cm}$ ; the linear dimensions of the short wave module are a factor of 1.3 smaller.

The simple spectrometer design employed here produces a moderate amount of anamorphic magnification, such that the image of a spectrally unresolved source is stretched in the dispersion direction by 20-50%. We will use a hexagonal array of pixels in which the pitch in the dispersion direction is naturally 15% larger than in the spatial direction, partially counteracting this anamorphism. The final imaging in the long wave module is at  $f/2.4$ , such that an image of a point source is 0.91mm in size. We design our hexagonal array of microlenses to have a pitch in the spatial direction of 1.18mm, such that we slightly undersample the spatial resolution element, and oversample the spectral resolution element. With a 25x64 pixel array we achieve an instantaneous bandwidth of  $\approx 14\%$  for each of the 25 spatial positions, and 2 grating settings (with the grating tipped by 5.5 degrees) are sufficient to cover the entire  $\approx 28\%$  band. The short wave module is imaged at  $f/3.3$  to maintain a constant image size, and the same array of hexagonally packed microlenses will be used to cover this band.

Both spectrometer modules are contained within a 1 K optical approximately cavity approximately 70 cm in diameter and 25 cm tall, painted black on the inside and using black baffles to control stray light and keep loading on the detectors low. Light enters this cavity after passing through low pass filters at 77K, 40K, and 4K, with a capacitive mesh bandpass filter at its entrance. IR blocking filters between each of the low pass filters cut down on the loading and increase the cryogen hold time. The total size of the spectrometer optics leads to a a cryostat of only slightly large overall size and cryogenic volume as the Z-Spec cryostat.

## 4.3. Kinetic-Inductance Detector (KID) Arrays

KIDs have emerged in the last decade as a straightforward approach to very large detector arrays for astrophysics. These devices rely on thin-film, high-Q micro-resonators that absorb incident radiation and respond by changing resonance frequency and line-width. These changes may be monitored by

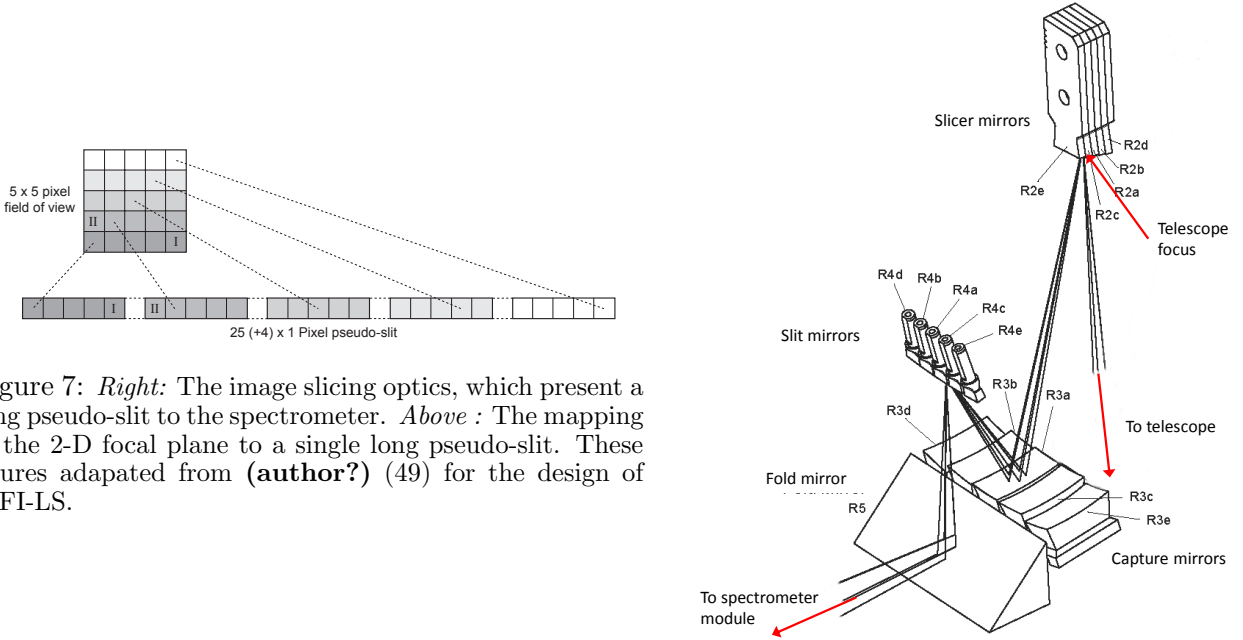


Figure 7: *Right*: The image slicing optics, which present a long pseudo-slit to the spectrometer. *Above* : The mapping of the 2-D focal plane to a single long pseudo-slit. These figures adapted from (author?) (49) for the design of FIFI-LS.

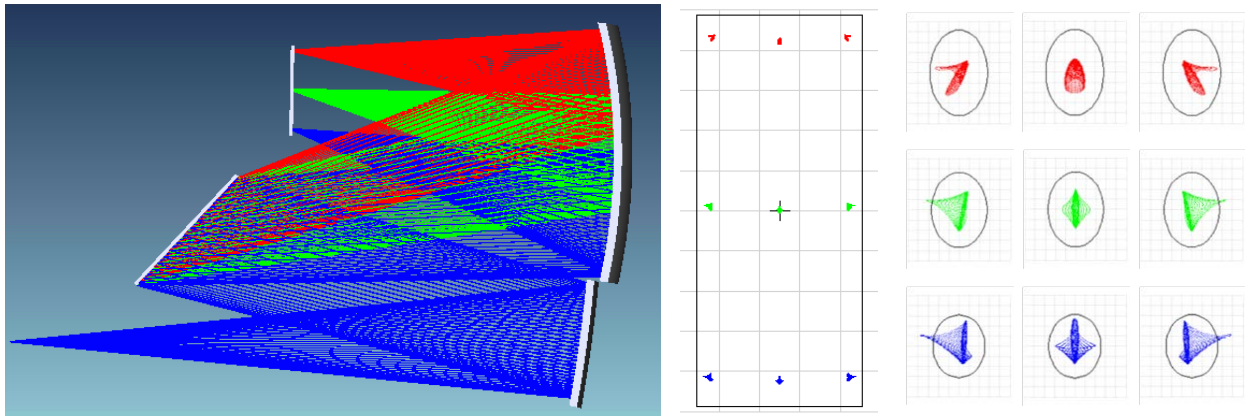


Figure 8: *Left*: The long wave spectrometer module showing the dispersion and imaging for 3 wavelengths spanning the instantaneous bandwidth. *Center*: Image of the array for the 3 wavelengths, and 3 field positions spanning the 25 pixel slit. *Right*: Geometric spot sizes for the 9 beams, compared with diffraction-limited Airy disk.

measuring the complex (amplitude and phase) transmission of an RF or microwave tone tuned to the resonance frequency. Due to the high resonance quality factors (narrow line widths) that can be achieved, large numbers of KIDs may be read out on a single RF/microwave feed line, and the only cryogenic electronics necessary is a single cold (4–20 K) RF/microwave amplifier per transmission line, which may be used for amplifying the signals of thousands of detectors.

KID technology is now approaching the performance levels of the SQUID-multiplexed bolometer systems in ground-based instruments. One example is the MUSIC camera now at the Caltech Submillimeter Observatory (CSO) (51) with participation from collaborator J. Zmuidzinas, with a total of 2304 detectors in 4 wavelength bands. Another is the dual-band 150/240 GHz, 224-pixel NIKA camera fielded at the IRAM 30-m telescope by European groups at SRON Utrecht (Baselmans), Institut NEEL (Benoit), and Cardiff (Doyle), which has demonstrated sensitivities approaching the photon background limit (52; 53; 54). KID technology has benefitted greatly from the Caltech / JPL discovery of the outstanding properties of titanium nitride (TiN) (55). TiN has a high normal state impedance,

making it easy to lithograph inductors into direct absorbers. It has intrinsically high Q values— $sQs$  as high as  $3 \times 10^7$  have been achieved with TiN resonators. These high Qs translate into the ability to build sensitive devices, and NEPs as low as  $4 \times 10^{-19} \text{ W Hz}^{-1/2}$  have been measured at Caltech / JPL, well below the ICARIS requirement of  $\text{NEP}_{\text{BG}} \sim 2 \times 10^{-18} \text{ W Hz}^{-1/2}$ . A final key feature of TiN is the ability to tune the  $T_c$  over a range from 0.8 to 4 K by varying film deposition conditions to tailor the response to a given application.

**Measured TiN KID Q and responsivity.** With these excellent properties demonstrated, TiN in lumped-element KIDs have become the focus of the Caltech / JPL effort, and our group has demonstrated the key properties of TiN KIDs through the 350- $\mu\text{m}$  MAKO camera development. First, we have shown that KIDs using TiN inductors provide Qs of  $10^5$  when operated at a base temperature of  $T_c/5$ , this sufficiently suppresses thermal quasiparticle excitations. Next, we have carefully measured the response of the TiN with the MAKO prototype arrays. The response of a given KID ( $\mathcal{R}_x$ ) is expressed as fractional frequency shift per input power ( $\delta f/f$  per W). However, the response is really due to changing the quasiparticle density in the inductor, so that with a given material and readout frequency, a KID system can be characterized by a fractional frequency response to *power density*:  $\mathcal{R}_V = \mathcal{R}_x \times V$  with units of  $(\delta f/f)/(W\mu\text{m}^{-3})$ . This volume-response product is the key materials parameter for specifying KIDs for lower-loading applications. KID responsivity can be increased by simply reducing the inductor volume.

**KID sensitivity and two-level system (TLS) noise.** The sensitivity of a KID is expressed as a ratio  $\text{NEP} = \sqrt{S_{xx}/\mathcal{R}_X}$ , where  $\mathcal{R}_x = \mathcal{R}_V/V$  is the response, as described above.  $S_{xx}$  is the variance in the fractional frequency fluctuations  $(\delta f/f)^2 \text{ Hz}^{-1}$ . The mechanism giving rise to  $S_{xx}$  in KIDs has been the subject of intense study by our group, and is now known to arise from fluctuations of the resonator capacitance due to the presence of microscopic two-level-system (TLS) fluctuators in amorphous dielectrics (56; 57; 58; 59; 60). The noise does *not* arise in the kinetic inductance detecting element itself, so it is possible to engineer the device to bring the TLS noise well below the fundamental photon noise. For ICARIS, as with MAKO and all of the current generation of KID systems, the first step is to bring the readout frequencies down from the microwave range (few GHz) into the RF range ( $\sim$  few 100 MHz) to achieve high  $Q$  (good muxing) with small volume (high responsivity) and to use cheaper, simpler electronics (see (61) for details). Another key parameter is the capacitor electrode spacing  $g$ , or pitch of the interdigitated capacitors: increasing the pitch reduces the electric field in the dielectric, reducing the noise according to  $S_{xx} \propto g^{-1.6}$ . Finally, we have developed a new pixel array architecture particularly well-suited to ICARIS and the other low-background applications in which all amorphous dielectric layers are eliminated. It consists of simply a single layer of TiN patterned on the crystalline silicon wafer (Figure 9). As Figure 9 shows,  $S_{xx}$  in this device is  $1.0 \times 10^{-18} \text{ Hz}^{-1}$ , a factor of 5–10 lower than the previous generation of devices using 2–3 metal layers and amorphous dielectric films. The MAKO prototype 350- $\mu\text{m}$  arrays are demonstrating in detail these sensitivity improvement; they are now clearly showing photon-noise-limited performance in laboratory measurements with 95% pixel yield.

**Pixel design for ICARIS.** ICARIS will use this single-layer architecture, and the same 100–250 MHz resonant frequencies as MAKO. It requires straightforward adjustments to accommodate the low loading and meet the required NEP. First, we will reduce the volume of the meandered inductor by a factor of 16, increasing its response by this same factor. The requirement to impedance match to the incident wave results in an invariant scaling between volume and area (a constant effective thickness), so that the volume reduction is also the area reduction. The ICARIS KID inductors will be patterned into circles of diameter 200  $\mu\text{m}$ . Coupling through a microlens array (described below) will preserve good focal-plane filling. The smaller inductor can provide the same total inductance, by simply meandering a smaller-width trace than (1.0  $\mu\text{m}$  wide instead of 2  $\mu\text{m}$ ) – our experience indicates that the failure rate is due to the total number of squares in the inductor, which is invariant since it scales as  $L$ , so

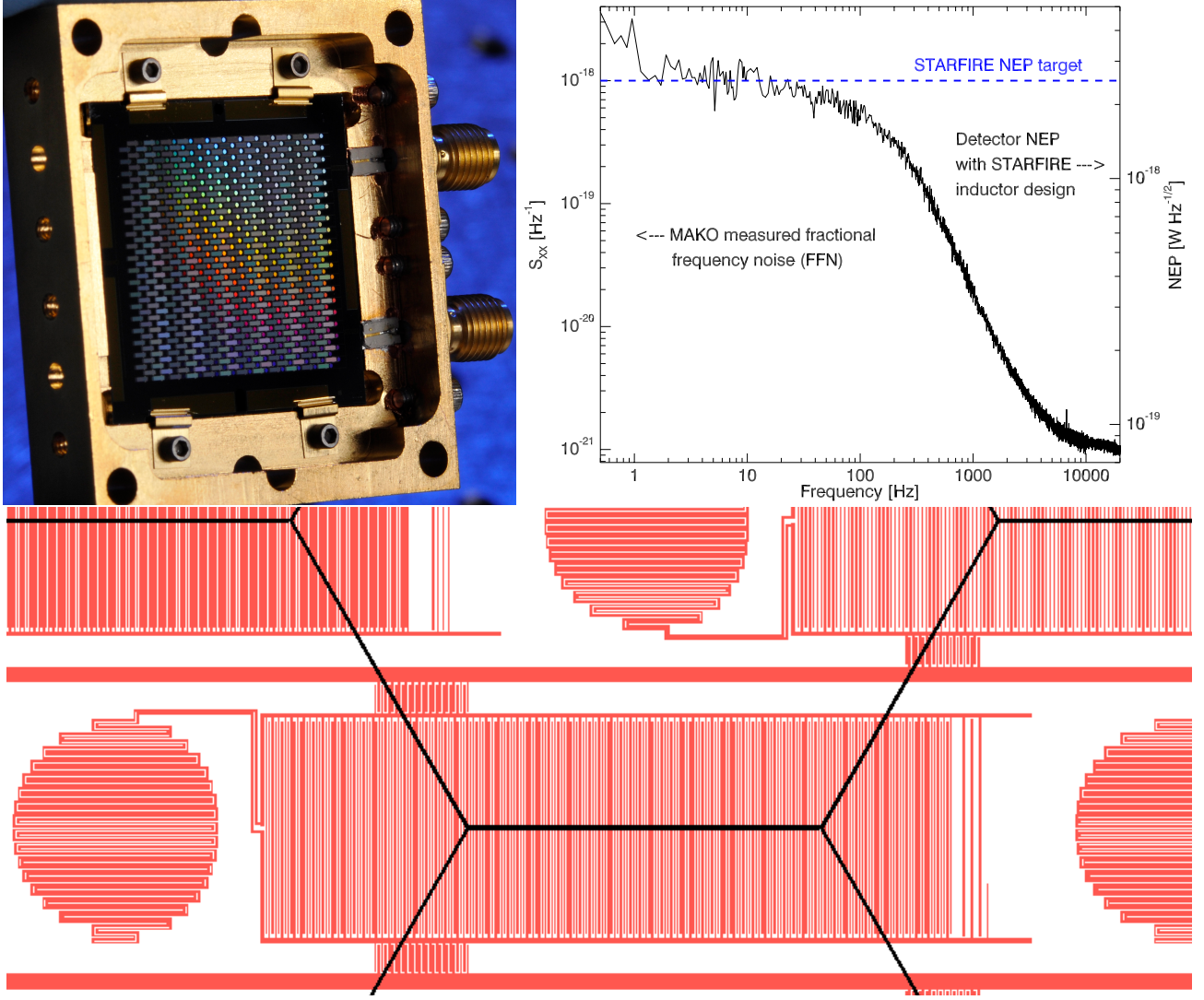


Figure 9: ICARIS lens-coupled TiN KID array architecture. Top, left shows a 432-pixel KID array (die is 22.5 mm on a side) for the MAKO 350- $\mu\text{m}$  ground-based camera. A similar array has demonstrated photon-noise limited performance in the lab and is en-route to the CSO as of this writing. Bottom shows the pixel detail. A single TiN layer forms the both the meandered inductors (circular features) and the interdigitated capacitors (rectangular features). The thick horizontal traces are the feed lines traversing the array (alternating polarity, so every other feedline is an effective ground). This pictured device has hexagonal packing (shown schematically in black) with a per-pixel area of 1 mm $^2$  (1.07 mm short hex spacing), and is tuned for MAKO loading. ICARIS will use a similar design with a slightly larger total pixel area (1.36 mm short hex spacing) but smaller circular inductor (200  $\mu\text{m}$  diameter instead of the pictured 350  $\mu\text{m}$  diameter). Top, right shows the fractional frequency noise measured in this device at 200 mK (left axis). The right-hand axis shows the inferred NEP which will be obtained with the inductor specified for ICARIS. The rolloff above 200 Hz shows the resonator bandwidth, ample for ICARIS. The rise below 1 Hz is due to a thermal drift in the stage temperature—it is unique to this measurement, and common across the array, so not relevant for ICARIS.

we anticipate high yield (>90%) as obtained with MAKO. Second, we will use a lower  $T_c$  TiN film, targeting 0.9 K instead of the 1.3 K used in MAKO. Since the response scales at least as  $T_c^{-2}$ , this provides a further factor of 2.1 increased response.  $T_c \sim 0.9$  K requires operation at  $T \sim 180$  mK, scaling from MAKO, but we baseline 150 mK to carry margin. This is readily achievable with high duty cycle with a commercial adiabatic demagnetization refrigerator (ADR).

To offset the increase in TLS noise due to the lower operating temperature, we will increase the electrode spacing  $g$ .  $\text{NEP}_{\text{TLS}} \propto \sqrt{S_{xx}} \propto T_{\text{op}}/g^{0.8}$ , so a factor of 1.4 increase in  $g$  is required to recover the measured TLS noise measured at 200 mK (Figure 9). The larger  $g$  reduces the capacitance slightly,

Figure 10: THIS FIGURE TO BE REPLACED WITH HORN ARRAY. Microlens arrays. TOP: 1-mm pitch lens array prototype machined from a silicon wafer by Veldlaser, with measured profile over several lenses shown at right. BOTTOM: f/0.8 microlens design for ICarIS, with hexagonal packing. This simulation is for a 1.5-mm diameter lens as an upper bound to the final lens size, in order demonstrate sufficient power concentration. HFSS simulations indicate 75% of the power incident in a uniform plane wave is coupled to the designed 200- $\mu\text{m}$  diameter inductor. The coupling to a more centrally-concentrated field distribution (such as the image of a point source centered on the pixel) will be higher.

but it can be compensated with an comparable increase in area, possible with our larger pixel pitch relative to the MAKO prototype. In any case, the impact on the KID resonant frequency is small ( $f = 1/\sqrt{LC}$ ), and the devices will still lie in our target readout band extending up to 250 MHz.

ICARIS will field 2 arrays, each with 64 (spectral)  $\times$  25 (spatial) = 1600 detectors, packed hexagonally with a 1.36-mm pitch. Each will require 2 readout chains, with  $\sim$ 800 channels each. The goal will be to field this on a single wafer-sized die, but mosaicing 2 dies into the package is a fallback option, producing only a small gap in the spectral direction which can moved away from lines of interest by tuning the grating. The package will provide a free-space  $\lambda/4$  backshort under the device wafer, as used in MAKO.

**Silicon microlens array.** Concentrating the radiation onto the small inductor requires a concentrating lens, and lens arrays have been designed and prototyped by our group. Figure 10 shows a prototype silicon lens array machined by Veldlaser (Heerenberg, Holland), as well as the measured profiles. While ICARIS requires somewhat greater concentration than these lenses, corresponding to a faster lens with greater curvature, this is not a problem for the laser manufacturing processes as arbitrary depths are possible. We have performed electromagnetic simulations to verify that good efficiency can be achieved coupling to the 200- $\mu\text{m}$ -diameter. (Figure 10). The lens is a hyperboloid with a total sag of 300  $\mu\text{m}$  (if sized at 1.5 mm), and it provides a total efficiency of >75%. To provide an anti-reflection (AR) coating, the lenses will be coated with a quarter-wavelength layer of parylene, a standard electronics packaging process. The microlens arrays will be simply clamped to the KID arrays, aligned using a pin and slot jig.

#### 4.4. Readouts

In order to achieve frequency domain multiplexing of KID arrays, two tasks must be accomplished: 1) A waveform consisting of a sum of frequency tones (each at an individual pixel frequency) must be generated and transmitted to the array and 2) after interacting with the pixels, the complex transmission of the individual tones must be extracted from the waveform. The first task is easily accomplished using a cyclic memory buffer and a DAC to continuously play back a pre-calculated periodic waveform. The second task can be accomplished using advanced digital-signal processing hardware. A fast, large-dynamic-range ADC is followed by a Field Programmable Gate Array (FPGA) which performs frequency separation utilizing a fast Fourier transform or more sophisticated techniques.

STARFIRE will use a multiplexing readout system developed by the Caltech / JPL group for 100–250 MHz KID arrays. This readout leverages the Reconfigurable Open Architecture Computing Hardware (ROACH) platform developed by the Berkeley CASPER group which features a Xilinx Virtex-5 FPGA. An additional daughter card provides two 1 GSPS DACs and two 500 MSPS ADCs. 500 MB of memory on the ROACH enables waveform playback by both DACs simultaneously. The readout uses custom FPGA firmware developed specifically for KID readout. The firmware implements a polyphase filter bank (PFB) to achieve an initial stage of coarse frequency separation. This is followed by multiplication of the PFB channels by pre-specified sinusoids and then low-pass filtering. This second stage allows fine-frequency separation of the waveform while avoiding calculation at frequencies containing no pixel information, resulting in a substantial savings of FPGA resources. This readout is working in the laboratory and is being deployed with the MAKO 350- $\mu\text{m}$  camera at the CSO telescope as of this writing. For the MAKO pixels, as will be the case for STARFIRE, the total noise from the cold amplifier and readout electronics is a comfortable factor of 3 lower (in  $S_{xx}$  units) than the noise from

the devices themselves. A single readout is capable of performing simultaneous complex transmission measurements of  $> 2000$  tones at a rate of 25 Hz, plenty of margin on the 800 detectors per readout chain we intend to use with STARFIRE.

Proper power budgeting requires understanding readout power consumption. A single roach board draws 86 W of power. Additionally, a readout computer is used to perform post-processing of the data and storage of the time stream. Conservatively, a single computer can service two ROACH systems. We can use computers optimized for lower power consumption. For 4 ROACH systems, we therefore estimate a power consumption of less than 500 W, a manageable figure, particularly for the short flights we envision.

#### 4.5. Telescope

The telescope design must be lightweight and compact, with low overall emissivity and high-efficiency coupling to the spectrometer. To reduce the emissivity, we have gone with an off-axis design which is nevertheless fairly compact and rigid. This led to an off-axis Gregorian design, with a parabolic primary with 2.5 m of projected aperture and an elliptical secondary. The secondary focus is located  $\sim 50$  cm behind the surface of the primary to allow plenty of room for backing structure, cryostat windows and filters. The maximum field of view (defined as when the beam at 300  $\mu\text{m}$  drops to a Strehl ratio of 0.95) is 0.5° in diameter. This is much larger than required for STARFIRE, and could be reused for other imaging submillimeter balloon missions.

The primary mirror will be machined of aluminum, similar to the mirror built for BLAST. The 1.8 meter BLAST mirror was re-made in 2009 by Magna Machining in Ohio. A diamond tool was used to machine the surface to an RMS of 0.45 microns with a form error less than 3.5 microns. We recently had this verified at L3-Brashear in Pittsburgh, PA. The larger primary proposed here will require further investigation to ensure it can be manufactured, but the technology is very similar to BLAST and ACT.

The secondary will be diamond turned by OASYS Technology (formerly Diamond Turning Inc.), the same company that machined the BLAST secondary mirror. By virtue of the off-axis design, the secondary support structure does not produce additional load on the detectors. However, the size and weight of the secondary has fundamental impact on the reliability of the pointing due to gravitational deflection of the secondary support. We have specified a very rigid support structure (see Figure 11, and will lightweight the secondary as much as possible.

Because of the different materials used for the mirrors and supports (aluminum and carbon fiber), the difference in the coefficient of thermal expansions would cause the telescope to go out of focus with changes in temperature. We will use the BLAST focusing system which has three precision actuators behind the secondary to provide 3 micron positioning (Figure 12). The entire system worked flawlessly during the BLAST 2006 flight.

In our sensitivity calculations and the parameters in Table 1, we have assumed that the temperature of the mirror is 250 K, the ambient air temperature at balloon float altitudes. Based on previous balloon missions (e.g., ? ), with sufficient high reflectivity baffling around the telescope, it can passively radiatively cool to 200 - 220 K, improving our sensitivity slightly. We also assume a 93% illumination for the primary.

#### 4.6. Cryogenics

The STARFIRE receiver consists of an optical cavity inside a long hold-time liquid-nitrogen and liquid-helium cryostat. Both the nitrogen and helium are maintained at slightly more than 15 psi during the flight to minimize loss due to pressure drop at altitude. A pumped pot maintains a 1 K stage with 20 mW of cooling power, which contains the entire spectrometer. The detectors are cooled with a series of pumped  $^3\text{He}/^4\text{He}$  sorption fridges, which back a commercially available adiabatic demagnetization refrigerator (ADR) to achieve a final temperature of 150 mK. A two-stage  $^3\text{He}$  refrigerator (designed and manufactured at Penn) provides a 300 mK sink during flight with 30  $\mu\text{W}$  of cooling power for



Figure 11: A Solidworks rendering of the STARFIRE telescope showing the off-axis optical design and the approximate size and location of the cryostat and star cameras. The Sun shields are not shown. The structure is based on the proven BLAST design. The frame will be made from carbon fiber and aluminum. The upper part of the gondola supporting the primary has been redesigned slightly from the BLAST architecture to support the larger off-axis 2.5 m mirror.

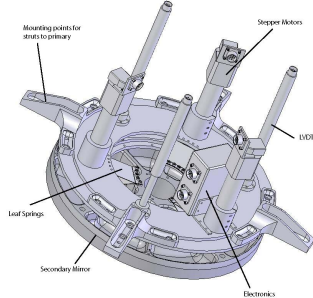


Figure 12: A rendering of the BLAST secondary positioning system. STARFIRE will use the same system to focus the off-axis secondary. The system was successfully tested during the BLAST Antarctic flight in 2006. It has tip/tilt and positional accuracy (in one dimension) of  $3 \mu\text{m}$ .

3 days. It is backed and cycled by a  $^4\text{He}$  stage. It can be recycled within 2 hrs. Our groups have built over ten receivers operating at temperatures from 50 to 300 mK, including an ADR for Z-Spec.

#### 4.7. Pointing and System

The STARFIRE gondola and pointing system is designed around the successful BLAST heritage. The gondola is shown in Figure 11. It consists of a precision-pointed inner frame (composed of the primary, secondary, near-field baffle, and cryostat) supported by an external gondola. The outer frame is pointed in azimuth by a flywheel and an active pivot. The inner frame has an elevation mount with direct-drive servo motors driving it relative to the outer frame. Balance of the inner frame is maintained by pumping liquid from the bottom of the frame to the top to compensate for cryogen boil-off.

The pointing system design is driven by the requirement of high in-flight accuracy, with an absolute accuracy of half a beam, and reconstructed accuracy  $<3''$ . The BLAST Antarctic flight obtained a pointing reconstruction of  $\approx 3''$  at  $1\sigma$  for small (1 degree) scans (43). The absolute in-flight pointing error was about  $1'$ . By improving the rigidity of the inner frame, and by not requiring large motions, we expect to be able to obtain better absolute in-flight pointing accuracy for STARFIRE.

The attitude determination system uses an array of pointing sensors including two sophisticated star cameras, two sets of fast, low-drift gyroscopes, a quad-GPS system, a digital Sun sensor, encoders, tilt sensors, and a magnetometer. The software is written to take full advantage of the abilities of each sensor in a hierarchical scheme where the fast, high-drift sensors (gyros) are continuously updated by the slower, absolute sensors (star cameras) and is robust against sensor failure. Optical encoders report the relative position of the inner frame to the outer frame. Motion sensing for the inner frame is provided by two sets of three orthogonally-mounted, high bandwidth gyroscopes.

The absolute pointing sensors are two integrating star cameras (62) that are mounted above the receiver on the inner frame. Each star camera has an internal computer that calculates a real-time pointing solution at 1 Hz by comparing measured star separations with an on-board catalog of stars.

The cameras are capable of dead reckoning. The two cameras run independently, providing failsafe redundancy. The camera system has been tested extensively on the ground and has flown four times on balloon payloads (three times on BLAST and once on the x-ray telescope InFOC $\mu$ S). A comparison of simultaneous pointing solutions from both cameras gives an rms uncertainty of  $<2''$ . To meet the absolute pointing requirements for STARFIRE, we will reduce the field of view of the cameras by a factor of two and use new CCDs with enhanced quantum efficiency that roughly doubles the sensitivity in the far red (where STARFIRE uses them). This will allow us to obtain high-accuracy, continuously updated pointing solutions for our observations.

## 5. FLIGHT OPERATIONS

We plan for two North American flights, each overnight, with a maximum flight time of approximately 24 hours, during which science data will be primarily acquired during the night. North American flights from Ft. Sumner, NM, or Palestine, TX, are typically scheduled in June or September to take advantage of “turnaround” wind conditions to produce the longest flight times. The availability of scientific targets strongly favors June for flights of STARFIRE. In June 2016, the planets Mars, Saturn, and Jupiter are available at modest elevation for calibration. The H-ATLAS fields at the NGP as well as GAMA12 and GAMA15 are available for pointed observations of lensed submillimeter galaxies in the early part of the night. Further north, well-studied small deep fields such as GOODS-N and the Groth Strip are available for long integrations testing the intensity mapping and stacking analyses.

The best launch opportunities occur at sunrise. We expect to be at float altitude at approximately 10 AM. This will give us 8 hours to cycle the fridges, check the detectors, and verify the pointing. The fridge hold times are sufficient that a single cycling at the beginning of the flight will hold for the entire flight. Science observations will begin at sunset. We anticipate 10 - 12 useful hours of science observations, including some after sunrise, in our calculations.

To establish the pointing initially, we will observe planets or other bright targets to establish the offset between the star cameras and the submillimeter optics. The accuracy of the mechanical alignment and the blind pointing solution from the star cameras should be better than  $2'$ , allowing the target to appear in the FOV created by the  $5 \times 5$  pixel array from the image slicer. A co-add of the spectral pixels will create a continuum image with high S/N. This offset will need to be periodically re-checked throughout the flight. These bright sources will also calibration of the PSF and focus checks for the secondary mirror.

For pointed observations, the two star cameras provide updates at 1 Hz. In between camera updates, the position is held based on the gyroscopes, the current generation of which on BLAST have drifts of  $1''/\text{second}$ . We will use improved versions with only  $0.05''/\text{second}$  drift, allowing extremely accurate maintained positions between star camera solution updates. This accuracy will be used to hold the target within the slicer FOV. The inevitable small motions around the nominal pointing center are actually advantageous as they modulate the target signal. The reconstructed position of the target within the focal plane will be better than a few arcseconds, allowing efficient coaddition of signal from the target. The off-target pixels as well as telluric-line-dominated spectral channels will be used to remove any effects of time-varying atmospheric emission.

For mapping observations, we will use a scan strategy similar to that of BLAST, with scans at fixed elevation while the FOV is moved back and forth in azimuth. The inner frame is then stepped to cover the entire field. In this mode, the scanning modulation helps to separate atmosphere and instrument drift to recover large scales in the image.

### 5.1. Scheduling

The flight software for STARFIRE will be designed so that it can operate autonomously after launch. However, because line-of-sight communication is maintained for the bulk of the flight, emergency changes can be implemented if necessary. The target fields will be decided before the flight. The autonomous scheduling system (developed for BLAST) will use schedule files that consist of a sequen-

tial list of observations or actions as a function of the Local Sidereal Time. This system is robust against temporary system failures because the telescope only needs to know the current time and location to resume operation upon recovery. Using a local sidereal clock rather than a clock fixed in some time zone, it is possible to account for purely astronomical visibility constraints (such as the RA of the Sun and of the astronomical targets) using a static description.

For every launch opportunity, six schedule files are generated, which account for 3 different cases flight latitude and longitude, and two cases of measured instrument sensitivity. The gondola uses the GPS to decide which schedule file to use, appropriate for the declination of the target field. Two sets of these three schedules are made: the first set assumes the instrument is working with the target sensitivities; the second assumes degradations of the telescope beam size by a factor of  $\sqrt{2}$ , and sensitivity by a factor of 2. At the beginning of the flight, the sensitivities and beam size are estimated from scans across calibrators. Based on this information the ground station team can decide which of the two sets of schedule files the instrument should use, and switch between the two using a single command.

## 5.2. In-Flight Data Operations

We will use several methods for primary calibration, most based on the successful approaches used by the direct-detection millimeter-wave spectrometer Z-Spec(e.g., (? ?)). The STARFIRE bands are sufficiently wide that a continuum calibrator can be used to calibrate both the absolute and relative response of the channels, and channels may also be co-added. Absolute calibration can be checked against the *Herschel*-SPIRE FTS measurements of the planets Mars (63) and Saturn (64).

For frequency calibration we will begin with a Fourier transform spectrometer (FTS) as a laboratory calibrator, as was done for Z-Spec. *Herschel*SPIRE FTS observations of evolved stars (65; 66) such as NGC 7027. A similar technique was used with great success for Z-Spec using IRC+10216. For STARFIRE, we have the additional frequency calibration scale of line emission from the atmosphere itself (since these lines will be narrow and do not suffer the severe pressure broadening present in ground-based observations).

The data rate from the STARFIRE detectors will be substantial, but not prohibitive. Each of the 6000 detectors will be sampled at a rate of 30 Hz, which, assuming 32 bit samples, is a rate of only 720 kB/s, or 2.6 GB per hour. Over the course of a 24 hour flight, this results in a total data volume of only  $\sim 70$  GB, including overheads for housekeeping data.

## 6. PLAN OF WORK

We recognize that STARFIRE will be a significant expense for the balloon program. In order to ensure that we are on-track with our technology and on-schedule to achieve our goals, we will have milestones and reviews by outside experts. We will organize external reviews of the two most critical and difficult aspects of the instrument: the spectrometer optics (including configuration and layout in the cryostat), and the detectors.

### 6.1. Schedule

**GY1: Oct 2013 - Sep 2014:** Our first year will be dominated by design and testing in preparation for Preliminary Design Review (PDR) in May and a Critical Design Review (CDR) in September. There will be separate PDRs and CDRs for the optics and detectors. While this is an aggressive schedule for these reviews, we need to prepare for a launch in the 4th year of the work.

JPL has already done a considerable amount of work on the detectors. An initial optics design has been completed. However, it will need to be optimized and the details of laying out the optics, detectors, and fridges in the cryostat which will need to be finalized.

**GY2 - 3: Oct 2014- Sep 2016:** These years will be dominated by building and testing all of the components of STARFIRE. JPL will begin the production of the first detectors as well as the detector package. Penn will work with the contractors to complete the telescope and gondola. In addition we

will construct the receiver, cryogenics, and cold optics. In the summer of 2016 we will integrate the instrument and prepare for mission readiness review.

**GY4: Oct 2016 - Sep 2017:** The first flight of STARFIRE is targeted for June 2017. Data reduction software will be in place, and reduction will begin promptly upon data acquisition.

**GY5: Oct 2017 - Sep 2018:** The final year of the grant is devoted to analysis of the data and a planned second flight in June 2017. We have a strong track record in analysis and releasing our data promptly to the community through the NASA IPAC archive.<sup>4</sup>

We have considered the reduction of risk throughout the process, largely by drawing on the proven BLAST heritage for the gondola and pointing. We also consider here several contingencies and options for descope. The STARFIREspectrometer design is highly modular. This allows for the possibility of excluding one or more modules from the flight instrument if there is a problem with the detectors or optics design. The impact on the science would be a reduction of the redshift range accessible.

## 6.2. Division of Labor and Personnel

To achieve the ambitious goals of this program, we have assembled a group of scientists with the wide range of backgrounds necessary to design, build and fly the instrument within the time scale described. Our team includes world leaders in advanced submillimeter detectors, background-limited (sub)millimeter spectroscopy, and scientific ballooning. Our team includes veterans from multiple balloon payloads (notably BLAST). We also have extensive experience with millimeter-wave spectrometers (Z-Spec), submillimeter receivers (ACT), and detector development (BLISS).

The project planning is a group effort coordinated by the PI at the University of Pennsylvania through frequent telecons and WWW-based information exchange. The University of Pennsylvania (Aguirre, Devlin) will build the receiver, telescope and gondola. JPL (Bradford) will supply the detectors and detector mounts. All collaborators will share in the data analysis. Close collaboration between the experimentalists, theorists and observers in our team will continue throughout the flight planning, field and source selection, and the analysis of the data. The entire team has been involved with the successful analysis of several large, complex CMB and submillimeter datasets and has an excellent history of prompt publication and distribution of data.

---

<sup>4</sup>See, for example:

<http://irsa.ipac.caltech.edu/Missions/bolocam.html> and  
<http://irsa.ipac.caltech.edu/Missions/blast.html>

Table 1: STARFIRE Instrument Parameters

<b>Telescope</b>					
Temperature	270K				
Diameter	1.8 m				
Illumination	0.93 (primary mirror is pupil stopped)				
Emissivity	0.04				
Primary $f/\#$	1.25				
Ritchey-Chretien $f/\#$	5				
<b>Detectors</b>					
TiN $T_c$	0.9 K				
Base temperature	250 mK				
KID resonator Q	$10^5$				
KID resonant frequencies	100–250 MHz				
MAKO pixel response	$1.2 \times 10^7 (\delta f/f) W^{-1}$ , measured				
ICARIS pixel response	$4 \times 10^8 (\delta f/f) W^{-1}$ , scaled from MAKO as $(\text{volume})^{-1}$ and $T_c^{-2}$				
$S_{xx}$ (due to TLS)	$1.0 \times 10^{-18} (\delta f/f)^2 \text{Hz}^{-1}$ , same as MAKO				
Detector efficiency w/ horns	65%				
Detector NEP (optical)	$2.5 \times 10^{-18} \text{W}/\sqrt{\text{Hz}}$				
$P_{absorbed}$	9 / 6 fW				
Photon NEP	$5.4/3.5 \times 10^{-18} \text{W}/\sqrt{\text{Hz}}$				
<b>Spectrometer</b>					
Format	2 modules, each 25 spatial $\times$ 64 spectral				
$R$	$450$ ( $670 \text{ km s}^{-1}$ )				
Optical efficiency	40%, exclusive of horn and detector				
	Short Wavelength		Long Wavelength		
Wavelength range	240 – 276	276 – 317	317 – 365	365 – 420	$\mu\text{m}$
$\Delta\nu$	2.58	2.25	1.95	1.70	GHz
Beam FWHM	25	29	34	39	"
Slit FOV	10.0	11.6	13.6	15.6	'
NEI	3.4	2.1	1.5	1.0	$\times 10^7 \text{ Jy sr}^{-1} \sqrt{\text{sec}}$
Line sensitivity	1.58	1.13	0.92	0.71	$\times 10^{-17} \text{ W m}^{-2} \sqrt{\text{sec}}$

## References

- [1] A. J. Benson. Galaxy formation theory. *Phys. Rep.*, 495:33–86, 2010.
- [2] J.-L. Puget, A. Abergel, J.-P. Bernard, F. Boulanger, W. B. Burton, F.-X. Desert, and D. Hartmann. Tentative detection of a cosmic far-infrared background with COBE . *A&A*, 308:L5+, 1996.
- [3] D. J. Fixsen, E. Dwek, J. C. Mather, C. L. Bennett, and R. A. Shafer. The Spectrum of the Extragalactic Far-Infrared Background from the COBE FIRAS Observations. *ApJ*, 508:123–128, 1998.
- [4] I. Smail, R. J. Ivison, and A. W. Blain. A Deep Sub-millimeter Survey of Lensing Clusters: A New Window on Galaxy Formation and Evolution. *ApJL*, 490:L5, 1997.
- [5] D. H. Hughes, S. Serjeant, J. Dunlop, M. Rowan-Robinson, A. Blain, R. G. Mann, R. Ivison, J. Peacock, A. Efstathiou, W. Gear, S. Oliver, A. Lawrence, M. Longair, P. Goldschmidt, and T. Jenness. High-redshift star formation in the Hubble Deep Field revealed by a submillimetre-wavelength survey. *Nature*, 394:241–247, 1998.
- [6] S. C. Chapman, A. W. Blain, I. Smail, and R. J. Ivison. A Redshift Survey of the Submillimeter Galaxy Population. *ApJ*, 622:772–796, 2005.
- [7] I. Artxaga, D. H. Hughes, K. Coppin, Á. M. J. Mortier, J. Wagg, J. S. Dunlop, E. L. Chapin, E. Eales, S. A. and Gaztañaga, M. Halpern, R. J. Ivison, E. van Kampen, D. Scott, S. Serjeant, T. Smail, I. and Babbedge, A. J. Benson, S. Chapman, D. L. Clements, L. Dunne, S. Dye, D. Farrah, M. J. Jarvis, R. G. Mann, A. Pope, R. Priddey, S. Rawlings, M. Seigar, L. Silva, C. Simpson, and M. Vaccari. The SCUBA Half Degree Extragalactic Survey - IV. Radio-mm-FIR photometric redshifts. *MNRAS*, 379:1571–1588, 2007.
- [8] E. Le Floc'h, C. Papovich, H. Dole, E. Egami, P. Perez-Gonzalez, G. Rieke, M. Rieke, E. Bell, and the Spitzer/MIPS GTO team. Evolution of the infrared luminosity density and star formation history up to  $z \sim 1$ : preliminary results from MIPS. *ArXiv Astrophysics e-prints*, 2004.
- [9] G. Lagache, J.-L. Puget, and H. Dole. Dusty Infrared Galaxies: Sources of the Cosmic Infrared Background. *ARAA*, 43:727–768, 2005.
- [10] B. T. Soifer and G. Neugebauer. The properties of infrared galaxies in the local universe. *Astron. J.*, 101:354–361, 1991.
- [11] A. M. Hopkins. The Star Formation History of the Universe. In J. Afonso, H. C. Ferguson, B. Mobasher, & R. Norris, editor, *Deepest Astronomical Surveys*, volume 380 of *Astronomical Society of the Pacific Conference Series*, pages 423–+. 2007.
- [12] J. D. Goldader, G. Meurer, T. M. Heckman, M. Seibert, D. B. Sanders, D. Calzetti, and C. C. Steidel. Far-Infrared Galaxies in the Far-Ultraviolet. *ApJ*, 568:651–678, 2002.
- [13] A. M. Swinbank, C. G. Lacey, I. Smail, C. M. Baugh, C. S. Frenk, A. W. Blain, S. C. Chapman, K. E. K. Coppin, R. J. Ivison, J. E. Gonzalez, and L. J. Hainline. The properties of submm galaxies in hierarchical models. *MNRAS*, 391:420–434, 2008.
- [14] I. Smail, R. J. Ivison, A. W. Blain, and J. -P. Kneib. The nature of faint submillimetre-selected galaxies. *MNRAS*, 331:495–520, 2002.
- [15] A. M. Swinbank, I. Smail, S. C. Chapman, A. W. Blain, R. J. Ivison, and W. C. Keel. The Rest-Frame Optical Spectra of SCUBA Galaxies. *ApJ*, 617:64–80, 2004.

- [16] A. W. Blain, S. C. Chapman, I. Smail, and R. Ivison. Clustering of Submillimeter-selected Galaxies. *ApJ*, 611:725–731, 2004.
- [17] A. Amblard, A. Cooray, P. Serra, B. Altieri, V. Arumugam, H. Aussel, A. Blain, J. Bock, A. Boselli, V. Buat, N. Castro-Rodríguez, A. Cava, P. Chanial, E. Chapin, D. L. Clements, A. Conley, L. Conversi, C. D. Dowell, E. Dwek, S. Eales, D. Elbaz, D. Farrah, A. Franceschini, W. Gear, J. Glenn, M. Griffin, M. Halpern, E. Hatziminaoglou, E. Ibar, K. Isaak, R. J. Ivison, A. A. Khostovan, G. Lagache, L. Levenson, N. Lu, S. Madden, B. Maffei, G. Mainetti, L. Marchetti, G. Marsden, K. Mitchell-Wynne, H. T. Nguyen, B. O'Halloran, S. J. Oliver, A. Omont, M. J. Page, P. Panuzzo, A. Papageorgiou, C. P. Pearson, I. Pérez-Fournon, M. Pohlen, N. Rangwala, I. G. Roseboom, M. Rowan-Robinson, M. S. Portal, B. Schulz, D. Scott, N. Seymour, D. L. Shupe, A. J. Smith, J. A. Stevens, M. Symeonidis, M. Trichas, K. Tugwell, M. Vaccari, E. Valiante, I. Valtchanov, J. D. Vieira, L. Vigroux, L. Wang, R. Ward, G. Wright, C. K. Xu, and M. Zemcov. Submillimetre galaxies reside in dark matter haloes with masses greater than  $3 \times 10^{11}$  solar masses. *Nature*, 470:510–512, 2011.
- [18] A. Cooray, A. Amblard, L. Wang, V. Arumugam, R. Auld, H. Aussel, T. Babbedge, A. Blain, J. Bock, A. Boselli, V. Buat, D. Burgarella, N. Castro-Rodriguez, A. Cava, P. Chanial, D. L. Clements, A. Conley, L. Conversi, C. D. Dowell, E. Dwek, S. Eales, D. Elbaz, D. Farrah, M. Fox, A. Franceschini, W. Gear, J. Glenn, M. Griffin, M. Halpern, E. Hatziminaoglou, E. Ibar, K. Isaak, R. J. Ivison, A. A. Khostovan, G. Lagache, L. Levenson, N. Lu, S. Madden, B. Maffei, G. Mainetti, L. Marchetti, G. Marsden, K. Mitchell-Wynne, A. M. J. Mortier, H. T. Nguyen, B. O'Halloran, S. J. Oliver, A. Omont, M. J. Page, P. Panuzzo, A. Papageorgiou, C. P. Pearson, I. Perez Fournon, M. Pohlen, J. I. Rawlings, G. Raymond, D. Rigopoulou, D. Rizzo, I. G. Roseboom, M. Rowan-Robinson, B. Schulz, D. Scott, P. Serra, N. Seymour, D. L. Shupe, A. J. Smith, J. A. Stevens, M. Symeonidis, M. Trichas, K. E. Tugwell, M. Vaccari, I. Valtchanov, J. D. Vieira, L. Vigroux, R. Ward, G. Wright, C. K. Xu, and M. Zemcov. HerMES: Halo occupation number and bias properties of dusty galaxies from angular clustering measurements. *A&A*, 518:L22, 2010.
- [19] E. Le Floc'h, C. Papovich, H. Dole, E. F. Bell, G. Lagache, G. H. Rieke, E. Egami, P. G. Pérez-González, A. Alonso-Herrero, M. J. Rieke, M. Blaylock, C. W. Engelbracht, K. D. Gordon, D. C. Hines, K. A. Misselt, J. E. Morrison, and J. Mould. Infrared Luminosity Functions from the Chandra Deep Field-South: The Spitzer View on the History of Dusty Star Formation at  $0 <^{\sim} z <^{\sim} 1$ . *ApJ*, 632:169–190, 2005.
- [20] M. J. Devlin, P. A. R. Ade, I. Arétxaga, J. J. Bock, E. L. Chapin, M. Griffin, J. O. Gundersen, M. Halpern, P. C. Hargrave, D. H. Hughes, J. Klein, G. Marsden, P. G. Martin, P. Mauskopf, L. Moncelsi, C. B. Netterfield, H. Ngo, L. Olmi, E. Pascale, G. Patanchon, M. Rex, D. Scott, C. Semisch, N. Thomas, M. D. P. Truch, C. Tucker, G. S. Tucker, M. P. Viero, and D. V. Wiebe. Over half of the far-infrared background light comes from galaxies at  $z >= 1.2$ . *Nature*, 458:737–739, 2009.
- [21] A. G. G. M. Tielens and D. Hollenbach. Photodissociation regions. I - Basic model. II - A model for the Orion photodissociation region. *ApJ*, 291:722–754, 1985.
- [22] G. J. Stacey, S. Hailey-Dunsheath, T. Ferkinhoff, C. an d Nikola, S. C. Parshley, D. J. Benford, J. G. Staguhn, and N. Fiolet. A  $158 \mu\text{m}$  [C II] Line Survey of Galaxies at  $z \sim 1-2$ : An Indicator of Star Formation in the Early Universe. *ApJ*, 724:957–974, 2010.
- [23] S. Hailey-Dunsheath, T. Nikola, G. J. Stacey, T. E. Oberst, S. C. Parshley, D. J. Benford, J. G. Staguhn, and C. E. Tucker. Detection of the  $158$  micron [CII] Transition at  $z=1.3$ : Evidence f or a Galaxy-Wide Starburst. *ArXiv e-prints* 1003.2174, 2010.

- [24] S. J. Curran. Ionised carbon and galaxy activity. *A&A*, 497:351–358, 2009.
- [25] M. L. Luhman, S. Satyapal, J. Fischer, M. G. Wolfire E. Sturm, C. C. Dudley, D. Lutz, and R. Genzel. The [C II] 158 Micron Line Deficit in Ultraluminous Infrared Galaxies Revisited. *ApJ*, 594:758–775, 2003.
- [26] T. M. Crawford, E. R. Switzer, W. L. Holzapfel, C. L. Reichardt, D. P. Marrone, and J. D. Vieira. A method for individual source brightness estimation in single- and multi-band millimeter-wave data. *ArXiv e-prints*, 0912.2341, 2009.
- [27] J. Graciá-Carpio, E. Sturm, S. Hailey-Dunsheath, J. Fischer, A. Contursi, A. Poglitsch, R. Genzel, E. González-Alfonso, A. Sternberg, A. Verma, N. Christopher, R. Davies, H. Feuchtgruber, J. A. de Jong, D. Lutz, and L. J. Tacconi. Far-infrared Line Deficits in Galaxies with Extreme L\_{FIR}/M\_{H\_2} Ratios. *ApJL*, 728:L7, 2011.
- [28] A. Boselli, G. Gavazzi, J. Lequeux, and D. Pierini. [CII] at 158 μm as a star formation tracer in late-type galaxies . *A&A*, 385:454–463, 2002.
- [29] I. de Looze, M. Baes, G. J. Bendo, L. Cortese, and J. Fritz. The reliability of [C II] as an indicator of the star formation rate. *MNRAS*, 416:2712–2724, 2011.
- [30] L. Sargsyan, V. Lebouteiller, D. Weedman, H. Spoon, J. Bernard-Salas, D. Engels, J. Stacey, G. and Houck, D. Barry, J. Miles, and A. Samsonyan. [C II] 158 μm Luminosities and Star Formation Rate in Dusty Starbursts and Active Galactic Nuclei. *ApJ*, 755:171, 2012.
- [31] Y. Gong, A. Cooray, M. Silva, M. G. Santos, J. Bock, C. M. Bradford, and M. Zemcov. Intensity Mapping of the [CII] Fine Structure Line during the Epoch of Reionization. *ArXiv e-prints* 1107.3553, 2011.
- [32] I. Valtchanov, J. Virdee, R. J. Ivison, B. Swinney, P. van der Werf, D. Rigopoulou, E. da Cunha, R. Lupu, D. J. Benford, D. Riechers, I. Smail, M. Jarvis, C. Pearson, H. Gomez, R. Hopwood, B. Altieri, M. Birkinshaw, D. Coia, L. Conversi, A. Cooray, G. de Zotti, L. Dunne, D. Frayer, L. Leeuw, A. Marston, M. Negrello, M. S. Portal, D. Scott, M. A. Thompson, M. Vaccari, M. Baes, D. Clements, M. J. Michałowski, H. Dannerbauer, S. Serjeant, R. Auld, S. Buttiglione, A. Cava, A. Dariush, S. Dye, S. Eales, J. Fritz, E. Ibar, S. Maddox, E. Pascale, M. Pohlen, E. Rigby, G. Rodighiero, D. J. B. Smith, P. Temi, J. Carpenter, A. Bolatto, M. Gurwell, and J. D. Vieira. Physical conditions of the interstellar medium of high-redshift, strongly lensed submillimetre galaxies from the Herschel-ATLAS. *MNRAS*, 415:3473–3484, 2011.
- [33] T.-C. Chang, U.-L. Pen, J. B. Peterson, and P. McDonald. Baryon Acoustic Oscillation Intensity Mapping of Dark Energy. *Physical Review Letters*, 100(9):091303, 2008.
- [34] T.-C. Chang, U.-L. Pen, K. Bandura, and J. B. Peterson. Hydrogen 21-cm Intensity Mapping at redshift 0.8. *ArXiv e-prints* 1007.3709, 2010.
- [35] C. L. Carilli. Intensity Mapping of Molecular Gas During Cosmic Reionization. *ApJL*, 730:L30, 2011.
- [36] A. Lidz, S. R. Furlanetto, S. P. Oh, J. Aguirre, T.-C. Chang, O. Doré, and J. R. Pritchard. Intensity Mapping with Carbon Monoxide Emission Lines and the Redshifted 21 cm Line. *ApJ*, 741:70, 2011.
- [37] Y. Gong, A. Cooray, M. B. Silva, M. G. Santos, and P. Lubin. Probing Reionization with Intensity Mapping of Molecular and Fine-structure Lines. *ApJL*, 728:L46, 2011.

- [38] E. Visbal, H. Trac, and A. Loeb. Demonstrating the feasibility of line intensity mapping using mock data of galaxy clustering from simulations. *J. Cosmology Astropart. Phys.*, 8:10, 2011.
- [39] E. Visbal and A. Loeb. Measuring the 3D clustering of undetected galaxies through cross correlation of their cumulative flux fluctuations from multiple spectral lines. *J. Cosmology Astropart. Phys.*, 11:16, 2010.
- [40] J. D. Bowman, M. F. Morales, and J. N. Hewitt. Foreground Contamination in Interferometric Measurements of the Redshifted 21 cm Power Spectrum. *ApJ*, 695:183–199, 2009.
- [41] M. F. Morales. Power Spectrum Sensitivity and the Design of Epoch of Reionization Observatories. *ApJ*, 619:678–683, 2005.
- [42] M. J. Devlin, P. A. R. Ade, I. Arétxaga, J. J. Bock, J. Chung, E. Chapin, S. R. Dicker, M. Griffin, J. Gundersen, M. Halpern, P. Hargrave, D. Hughes, J. Klein, G. Marsden, P. Martin, P. D. Mauskopf, B. Netterfield, L. Olmi, E. Pascale, M. Rex, D. Scott, C. Semisch, M. Truch, C. Tucker, G. Tucker, A. D. Turner, and D. Weibe. The Balloon-borne Large Aperture Submillimeter Telescope (BLAST). In *Astronomical Structures and Mechanisms Technology. Edited by Antebi, Joseph; Lemke, Dietrich. Proceedings of the SPIE, Volume 5498, pp. 42-54 (2004).*, pages 42–54, 2004.
- [43] E. Pascale, P. A. R. Ade, J. J. Bock, E. L. Chapin, J. Chung, M. J. Devlin, S. Dicker, M. Griffin, J. O. Gundersen, M. Halpern, P. C. Hargrave, D. H. Hughes, J. Klein, C. J. MacTavish, G. Marsden, P. G. Martin, T. G. Martin, P. Mauskopf, C. B. Netterfield, L. Olmi, G. Patanchon, M. Rex, D. Scott, C. Semisch, N. Thomas, M. D. P. Truch, C. Tucker, G. S. Tucker, M. P. Viero, and D. V. Wiebe. The Balloon-borne Large Aperture Submillimeter Telescope: BLAST. *ApJ*, 681:400–414, 2008.
- [44] H. Inami, M. Bradford, J. Aguirre, L. Earle, B. Naylor, H. Matsuhara, J. Glenn, H. Nguyen, J. J. Bock, J. Zmuidzinas, and Y. Ohyama. A broadband millimeter-wave spectrometer Z-spec: sensitivity and ULIRGs. In *Society of Photo-Optical Instrumentation Engineers (SPIE) Conference Series*, volume 7020 of *Society of Photo-Optical Instrumentation Engineers (SPIE) Conference Series*, 2008.
- [45] L. Earle, P. Ade, J. Aguirre, R. Aikin, J. Battle, J. Bock, C. M. Bradford, M. Dragovan, L. Duband, J. Glenn, G. Griffin, V. Hristov, P. Maloney, H. Matsuhara, B. Naylor, H. Nguyen, M. Yun, and J. Zmuidzinas. Z-Spec: a broadband direct-detection millimeter-wave spectrometer -instrument status and first results. In *Millimeter and Submillimeter Detectors and Instrumentation for Astronomy III. Edited by Zmuidzinas, Jonas; Holland, Wayne S.; Withington, Stafford; Duncan, William D.. Proceedings of the SPIE, Volume 6275, pp. 627510 (2006).*, volume 6275 of *Presented at the Society of Photo-Optical Instrumentation Engineers (SPIE) Conference*, 2006.
- [46] C. M. Bradford, P. Ade, J. Aguirre, J. J. Bock, M. Dragovan, L. Duband, L. Earle, J. Glenn, H. Matsuhara, B. J. Naylor, H. Nguyen, M. Yun, and J. Zmuidzinas. Z-Spec: a broadband millimeter-wave grating spectrometer — design, construction, and first cryogenic measurements. In *Millimeter and Submillimeter Detectors for Astronomy II*, volume 5498 of *Proc. SPIE*, pages 257–267, 2004.
- [47] C. M. Bradford, B. J. Naylor, J. Zmuidzinas, J. J. Bock, J. Gromke, H. Nguyen, M. Dragovan, M. Yun, L. Earle, J. Glenn, H. Matsuhara, P. A. R. Ade, and L. Duband. WaFIRS: a waveguide far-IR spectrometer: enabling spectroscopy of high-z galaxies in the far-IR and submillimeter. In *IR Space Telescopes and Instruments*, volume 4850 of *Proc. SPIE*, pages 1137–1148, 2003.

- [48] B. J. Naylor, P. A. R. Ade, J. J. Bock, C. M. Bradford, M. Dragovan, L. Duband, L. Earle, J. Glenn, H. Matsuhara, H. Nguyen, M. Yun, and J. Zmuidzinas. Z-Spec: a broadband, direct-detection, millimeter-wave spectrometer. In *Millimeter and Submillimeter Detectors for Astronomy*, volume 4855 of *Proc. SPIE*, pages 239–248, 2003.
- [49] L. W. Looney, W. Raab, A. Poglitsch, and N. Geis. Realizing Integral Field Spectroscopy in the Far-Infrared. *ApJ*, 597:628–643, 2003.
- [50] L. W. Looney, W. Raab, A. Poglitsch, N. Geis, D. Rosenthal, R. Hoenle, R. Klein, F. Fumi, R. Genzel, and T. Henning. FIFI LS: a far-infrared 3D spectral imager for SOFIA. In R. K. Melugin and H.-P. Roeser, editors, *Society of Photo-Optical Instrumentation Engineers (SPIE) Conference Series*, volume 4857 of *Society of Photo-Optical Instrumentation Engineers (SPIE) Conference Series*, pages 47–55, 2003.
- [51] James A. Schlaerth, Nicole G. Czakon, Peter K. Day, Thomas P. Downes, Ran Duan, Jiansong Gao, Jason Glenn, Sunil R. Golwala, Matthew I. Hollister, Henry G. LeDuc, Benjamin A. Mazin, Philip R. Maloney, Omid Noroozian, Hien T. Nguyen, Jack Sayers, Seth Siegel, John E. Vaillancourt, Anastasios Vayonakis, Philip R. Wilson, and Jonas Zmuidzinas. MKID multicolor array status and results from DemoCam. In Holland, WS and Zmuidzinas, J, editor, *MILLIMETER, SUBMILLIMETER, AND FAR-INFRARED DETECTORS AND INSTRUMENTATION FOR ASTRONOMY V*, volume 7741 of *Proceedings of SPIE-The International Society for Optical Engineering*, 1000 20TH ST, PO BOX 10, BELLINGHAM, WA 98227-0010 USA, 2010. SPIE, SPIE-INT SOC OPTICAL ENGINEERING. Conference on Millimeter, Submillimeter, and Far-Infrared Detectors and Instrumentation for Astronomy V, San Diego, CA, JUN 29-JUL 02, 2010.
- [52] A. Monfardini, A. Benoit, A. Bideaud, L. Swenson, A. Cruciani, P. Camus, C. Hoffmann, F. X. Désert, S. Doyle, P. Ade, P. Mauskopf, C. Tucker, M. Roesch, S. Leclercq, K. F. Schuster, A. Endo, A. Baryshev, J. J. A. Baselmans, L. Ferrari, S. J. C. Yates, O. Bourrion, J. Macias-Perez, C. Vescovi, M. Calvo, and C. Giordano. A Dual-band Millimeter-wave Kinetic Inductance Camera for the IRAM 30 m Telescope. *ApJS*, 194:24–+, 2011.
- [53] S. J. C. Yates, J. J. A. Baselmans, A. Endo, R. M. J. Janssen, L. Ferrari, P. Diener, and A. M. Baryshev. Photon noise limited radiation detection with lens-antenna coupled Microwave Kinetic Inductance Detectors. *ArXiv e-prints 1107.4330*, 2011.
- [54] M. Calvo, M. Roesch, F.-X. Désert, A. Monfardini, A. Benoit, P. Mauskopf, P. Ade, N. Boudou, O. Bourrion, P. Camus, A. Cruciani, S. Doyle, C. Hoffmann, S. Leclercq, J. F. Macias-Perez, N. Ponthieu, K. F. Schuster, C. Tucker, and C. Vescovi. Improved mm-wave photometry for kinetic inductance detectors. *A&A*, 551:L12, 2013.
- [55] Henry G. Leduc, Bruce Bumble, Peter K. Day, Byeong Ho Eom, Jiansong Gao, Sunil Golwala, Benjamin A. Mazin, Sean McHugh, Andrew Merrill, David C. Moore, Omid Noroozian, Anthony D. Turner, and Jonas Zmuidzinas. Titanium nitride films for ultrasensitive microresonator detectors. *APPLIED PHYSICS LETTERS*, 97(10), 2010.
- [56] Jiansong Gao, Jonas Zmuidzinas, Benjamin A. Mazin, Henry G. LeDuc, and Peter K. Day. Noise properties of superconducting coplanar waveguide microwave resonators. *Applied Physics Letters*, 90(10):102507, 2007.
- [57] Shwetank Kumar, Jiansong Gao, Jonas Zmuidzinas, Benjamin A. Mazin, Henry G. LeDuc, and Peter K. Day. Temperature dependence of the frequency and noise of superconducting coplanar waveguide resonators. *Applied Physics Letters*, 92(12):123503, 2008.

- [58] Jiansong Gao, Miguel Daal, Anastasios Vayonakis, Shwetank Kumar, Jonas Zmuidzinas, Bernard Sadoulet, Benjamin A. Mazin, Peter K. Day, and Henry G. Leduc. Experimental evidence for a surface distribution of two-level systems in superconducting lithographed microwave resonators. *Applied Physics Letters*, 92(15):152505, 2008.
- [59] Jiansong Gao, Miguel Daal, John M. Martinis, Anastasios Vayonakis, Jonas Zmuidzinas, Bernard Sadoulet, Benjamin A. Mazin, Peter K. Day, and Henry G. Leduc. A semiempirical model for two-level system noise in superconducting microresonators. *Applied Physics Letters*, 92(21):212504, 2008.
- [60] Omid Noroozian, Jiansong Gao, Jonas Zmuidzinas, Henry G. LeDuc, and Benjamin A. Mazin. Two-level system noise reduction for microwave kinetic inductance detectors. *AIP Conference Proceedings*, 1185(1):148–151, 2009.
- [61] Jonas Zmuidzinas. Superconducting microresonators: Physics and applications. *Annual Review of Condensed Matter Physics*, 3(1):169–214, 2012.
- [62] M. Rex, E. Chapin, M. J. Devlin, J. Gundersen, J. Klein, E. Pascale, and D. Wiebe. BLAST autonomous daytime star cameras. In *Ground-based and Airborne Instrumentation for Astronomy. Edited by McLean, Ian S.; Iye, Masanori. Proceedings of the SPIE, Volume 6269, pp. 62693H (2006).*, volume 6269 of *Presented at the Society of Photo-Optical Instrumentation Engineers (SPIE) Conference*, 2006.
- [63] B. M. Swinyard, P. Hartogh, S. Sidher, T. Fulton, E. Lellouch, C. Jarchow, M. J. Griffin, R. Moreno, H. Sagawa, G. Portyankina, M. Blecka, M. Banaszkiewicz, D. Bockele-Morvan, J. Crovisier, T. Encrenaz, M. Kueppers, L. Lara, D. Lis, A. Medvedev, M. Rengel, S. Szutowicz, B. Vandenbussche, F. Bensch, E. Bergin, F. Billebaud, N. Biver, G. Blake, J. Blommaert, M. de Val-Borro, J. Cernicharo, T. Cavalie, R. Courtin, G. Davis, L. Decin, P. Encrenaz, T. de Graauw, E. Jehin, M. Kidger, S. Leeks, G. Orton, D. Naylor, R. Schieder, D. Stam, N. Thomas, E. Verdugo, C. Waelkens, and H. Walker. The Herschel-SPIRE submillimetre spectrum of Mars. *A&A*, 518:L151, 2010.
- [64] L. N. Fletcher, B. Swinyard, C. Salji, E. Polehampton, T. Fulton, S. Sidher, E. Lellouch, R. Moreno, G. Orton, T. Cavalié, R. Courtin, M. Rengel, H. Sagawa, G. R. Davis, P. Hartogh, D. Naylor, H. Walker, and T. Lim. Sub-millimetre spectroscopy of Saturn’s trace gases from Herschel/SPIRE. *A&A*, 539:A44, 2012.
- [65] M. A. T. Groenewegen, C. Waelkens, M. J. Barlow, F. Kerschbaum, P. Garcia-Lario, J. Cernicharo, J. A. D. L. Blommaert, J. Bouwman, M. Cohen, N. Cox, L. Decin, K. Exter, W. K. Gear, H. L. Gomez, P. C. Hargrave, T. Henning, D. Hutsemékers, R. J. Ivison, A. Jorissen, O. Krause, D. Ladjal, S. J. Leeks, T. L. Lim, M. Matsuura, Y. Nazé, G. Olofsson, R. Ottensamer, E. Polehampton, T. Posch, G. Rauw, P. Royer, B. Sibthorpe, B. M. Swinyard, T. Ueta, C. Vamvatira-Nakou, B. Vandenbussche, G. C. van de Steene, S. van Eck, P. A. M. van Hoof, H. van Winckel, E. Verdugo, and R. Wesson. MESS (Mass-loss of Evolved StarS), a Herschel key program. *A&A*, 526:A162, 2011.
- [66] R. Wesson, J. Cernicharo, M. J. Barlow, M. Matsuura, L. Decin, M. A. T. Groenewegen, E. T. Polehampton, M. Agundez, M. Cohen, F. Daniel, K. M. Exter, W. K. Gear, H. L. Gomez, P. C. Hargrave, P. Imhof, R. J. Ivison, S. J. Leeks, T. L. Lim, G. Olofsson, G. Savini, B. Sibthorpe, B. M. Swinyard, T. Ueta, D. K. Witherick, and J. A. Yates. Herschel-SPIRE FTS Spectroscopy of Evolved Stars. In F. Kerschbaum, T. Lebzelter, and R. F. Wing, editors, *Why Galaxies Care about AGB Stars II: Shining Examples and Common Inhabitants*, volume 445 of *Astronomical Society of the Pacific Conference Series*, page 607, 2011.

**James E. Aguirre**  
**Professional Preparation**

Georgia Institute of Technology	Physics / Applied Mathematics	BS 1997
University of Chicago	Physics	PhD 2003
University of Colorado, Boulder	Postdoctoral Research Associate	2003 - 2005
National Radio Astronomy Observatory	Jansky Postdoctoral Fellow	2003 - 2008

**Appointments**

Assistant Professor, Department of Physics and Astronomy, University of Pennsylvania, 2008 -  
Jansky Fellow, National Radio Astronomy Observatory, 2005 - 2008  
Postdoctoral Research Associate, University of Colorado, Boulder, 2003 - 2005  
Graduate Research Assistant, University of Chicago, Department of Physics, 1997 - 2003  
National Science Foundation Graduate Research Fellow, awarded 1997.

**Projects and Grants**

- PI of NSF Astronomy and Astrophysics Grant AST-0807990 “Broadband Millimeter Spectroscopy with Z-Spec: Molecular Diagnostics of Local ULIRGs and Redshifts for Submillimeter Galaxies”, 7/1/2008 - 6/30/2011, \$426,977
- PI of University of Pennsylvania Research Foundation Grant “A Cryogenic Testbed for Advanced Millimeter-Wave Astronomical Detectors”, 7/27/2009- 6/31/2010, \$50,000
- PI of Mt. Cuba Astronomical Foundation Grant “An Advanced Data Handling System to Enable the Detection of the Epoch of Reionization”, \$100,000
- Co-I of NSF Astronomy and Astrophysics Grant AST-1007905 “High Resolution Observations of the Sunyaev-Zel'dovich Effect in Clusters of Galaxies and High-z Galaxies at 90 GHz Using the GBT” (PI M. Devlin) 7/1/2010 - 6/30/2012, \$545,561
- Co-I and Executive Committee member for the NSF grant AST 1125558 “Collaborative Research: Precision Array for Probing the Epoch of Reionization (PAPER)”, a joint venture with University of California Berkeley, and NRAO / University of Virginia

**Relevant Publications**

- C. M. Bradford, A. D. Bolatto, P. R. Maloney, J. E. **Aguirre**, J. J. Bock, J. Glenn, J. Kamenetzky, R. Lupu, H. Matsuhara, E. J. Murphy, B. J. Naylor, H. T. Nguyen, K. Scott, and J. Zmuidzinas. The Water Vapor Spectrum of APM 08279+5255: X-Ray Heating and Infrared Pumping over Hundreds of Parsecs. ApJL, 741:L37+, 2011.
- A. Lidz, S. R. Furlanetto, S. P. Oh, J. **Aguirre**, T.-C. Chang, O. Doré, and J. R. Pritchard. Intensity Mapping with Carbon Monoxide Emission Lines and the Redshifted 21 cm Line. ApJ, 741:70+, 2011.
- K. S. Scott, R. E. Lupu, J. E. **Aguirre**, R. Auld, H. Aussel, A. J. Baker, A. Beelen, J. Bock, C. M. Bradford, D. Brisbin, D. Burgarella, J. M. Carpenter, P. Chanial, S. C. Chapman, D. L. Clements, A. Conley, A. Cooray, P. Cox, C. D. Dowell, S. Eales, D. Farrah, A. Franceschini, D. T. Frayer, R. Gavazzi, J. Glenn, M. Griffin, A. I. Harris, E. Ibar, R. J. Ivison, J. Kamenetzky, S. Kim, M. Krips, P. R. Maloney, H. Matsuhara, A. M. J. Mortier, E. J. Murphy, B. J. Naylor, R. Neri, H. T. Nguyen, S. J. Oliver, A. Omont, M. J. Page, A. Papageorgiou, C. P. Pearson, I. Pérez-Fournon, M. Pohlen, J. I. Rawlings, G. Raymond, D. Riechers, G. Rodighiero, I. G. Roseboom, M. Rowan-Robinson, D. Scott, N. Seymour, A. J. Smith, M. Symeonidis, K. E. Tugwell, M. Vaccari, J. D. Vieira, L. Vigroux, L. Wang, G. Wright, and J. Zmuidzinas. Redshift Determination and CO Line Excitation Modeling for the Multiply Lensed Galaxy HLSW-01. ApJ, 733:29+, 2011

M. Negrello, R. Hopwood, G. De Zotti, A. Cooray, A. Verma, J. Bock, D. T. Frayer, M. A. Gurwell, A. Omont, R. Neri, H. Dannerbauer, L. L. Leeuw, E. Barton, J. Cooke, S. Kim, E. da Cunha, G. Rodighiero, P. Cox, D. G. Bonfield, M. J. Jarvis, S. Serjeant, R. J. Ivison, S. Dye, I. Arétxaga, D. H. Hughes, E. Ibar, F. Bertoldi, I. Valtchanov, S. Eales, L. Dunne, S. P. Driver, R. Auld, S. Buttiglione, A. Cava, C. A. Grady, D. L. Clements, A. Dariush, J. Fritz, D. Hill, J. B. Hornbeck, L. Kelvin, G. Lagache, M. Lopez-Caniego, J. Gonzalez-Nuevo, S. Maddox, E. Pascale, M. Pohlen, E. E. Rigby, A. Robotham, C. Simpson, D. J. B. Smith, P. Temi, M. A. Thompson, B. E. Woodgate, D. G. York, J. E. **Aguirre**, A. Beelen, A. Blain, A. J. Baker, M. Birkinshaw, R. Blundell, C. M. Bradford, D. Burgarella, L. Danese, J. S. Dunlop, S. Fleuren, J. Glenn, A. I. Harris, J. Kamenetzky, R. E. Lupu, R. J. Maddalena, B. F. Madore, P. R. Maloney, H. Matsuhara, M. J. Michaowski, E. J. Murphy, B. J. Naylor, H. Nguyen, C. Popescu, S. Rawlings, D. Rigopoulou, D. Scott, K. S. Scott, M. Seibert, I. Smail, R. J. Tuffs, J. D. Vieira, P. P. van der Werf, and J. Zmuidzinas. The Detection of a Population of Submillimeter-Bright, Strongly Lensed Galaxies. *Science*, 330:800–, 2010.

C. M. Bradford, J. E. **Aguirre**, R. Aikin, J. J. Bock, L. Earle, J. Glenn, H. Inami, P. R. Maloney, H. Matsuhara, B. J. Naylor, H. T. Nguyen, and J. Zmuidzinas. The Warm Molecular Gas around the Cloverleaf Quasar. *ApJ*, 705:112–122, 2009.

J. Kamenetzky, J. Glenn, P. R. Maloney, J. E. **Aguirre**, J. J. Bock, C. M. Bradford, L. Earle, H. Inami, H. Matsuhara, E. J. Murphy, B. J. Naylor, H. T. Nguyen, and J. Zmuidzinas. The Dense Molecular Gas in the Circumnuclear Disk of NGC 1068. *ApJ*, 731:83–, 2011.

B. J. Naylor, C. M. Bradford, J. E. **Aguirre**, J. J. Bock, L. Earle, J. Glenn, H. Inami, J. Kamenetzky, P. R. Maloney, H. Matsuhara, H. T. Nguyen, and J. Zmuidzinas. A Census of the High-density Molecular Gas in M82. *ApJ*, 722:668–681, 2010.

## Additional Publications

J. E. **Aguirre**, A. G. Ginsburg, M. K. Dunham, M. M. Drosback, J. Bally, C. Battersby, E. T. Bradley, C. Cyganowski, D. Dowell, N. J. Evans, II, J. Glenn, P. Harvey, E. Rosolowsky, G. S. Stringfellow, J. Walawender, and J. P. Williams. The Bolocam Galactic Plane Survey: Survey Description and Data Reduction. *ApJS*, 192:4–, 2011.

M. Lima, B. Jain, M. Devlin, and J. **Aguirre**. Submillimeter Galaxy Number Counts and Magnification by Galaxy Clusters. *ApJL*, 717:L31–L36, 2010.

D. C. Jacobs, J. E. **Aguirre**, A. R. Parsons, J. C. Pober, R. F. Bradley, C. L. Carilli, N. E. Gugliucci, J. R. Manley, C. van der Merwe, D. F. Moore, and C. R. Parashare. New 145 MHz Source Measurements by PAPER in the Southern Sky. *ApJL*, 734:L34+, 2011.

A. Parsons, M. McQuinn, D. Jacobs, J. **Aguirre**, and J. Pober. A Sensitivity and Array - Configuration Study for Measuring the Power Spectrum of 21cm Emission from Reionization. *Provisional acceptance by ApJ; ArXiv e-prints* 1103.2135, 2011.

A. R. Parsons, D. C. Backer, G. S. Foster, M. C. H. Wright, R. F. Bradley, N. E. Gugliucci, C. R. Parashare, E. E. Benoit, J. E. **Aguirre**, D. C. Jacobs, C. L. Carilli, D. Herne, M. J. Lynch, J. R. Manley, and D. J. Werthimer. The Precision Array for Probing the Epoch of Re-ionization: Eight Station Results. *Astron. J.*, 139:1468–1480, 2010.

## Synergistic Activities

- Reviewer for NASA Astrophysics Theory Program 2009 • Developed and taught a one week course in radio astronomy for the Penn Summer Science Academy (PSSA), 2010 and 2011 • Public lectures to NRAO Pulsar Collaboratory and PSSA • Reviewer for MNRAS • US panelist for a scientific review proposed instrument suite the Japanese satellite SPICA

## Budget Justification

This proposal asks for funds to design, build, and fly STARFIRE and analyze its data. We already have extensive infrastructure from BLAST for support in the field. The STARFIRE gondola and flight electronics are clones of the proven BLAST design. We believe it will take three years to design and build the payload with overnight North American flights in the fourth and fifth year, with analysis promptly after the flights. The total amount of data will be modest, and flying later will allow the reduction pipeline to be more fully developed.

A large fraction of our budget goes to JPL to design, develop and build the detectors. The STARFIRE detector development program will make possible a future balloon mission competitive with satellites, as well as provide dividends for future space missions and benefit the community generally. The Penn budget includes JPL as a subcontract; however as a NASA center, these funds are allocated directly. The JPL budget is included as a separate spreadsheet.

- **Personnel** We have a number of very experienced people working on STARFIRE, and will train new postdocs and graduate students.
  - Jeff Klein has functioned as the project scientist for BLAST since its inception. He is universally accepted within the collaboration as an indispensable member of the team. His knowledge base supports the entire project. Through his work on ACT he has also become an expert with the TES detectors and most importantly the multiplexing electronics. He is supported 2 months/year on STARFIRE during the final three years of the grant to support integration and field work.
  - Simon Dicker has been a scientist at Penn for more than 10 years. He designed, built, and fielded the first array of bolometers on the Green Bank Telescope. He has extensive experience with optical design and TES detectors. He is supported during the initial portion of the award to work on optical and cryogenic design, and has already begun designing the spectrometer and telescope optics.
  - We will hire two postdocs at Penn to help design and build the many new components for STARFIRE, as well as a postdoc through the JPL subcontract. We have included the biographical sketch of Steve Hailey-Dunsheath, who has expressed an interest in the proposal and contributed to it.
  - There will be two new graduate students at Penn. With the help of our experienced staff and postdocs, these students will be coming up to speed on the STARFIRE instrument to help support the next generation of experiments. They will also work on specialized data planning and analysis. Aguirre currently has one student who will help train the new students: Bade Uzgil, partially supported by a NASA GSRP has been doing theoretical calculations in intensity mapping.
  - Undergraduates have been involved with all of our projects (over 50 in the last 10 years). They have worked closely with our team to help to build and support the instruments. Most move on to graduate school. Some are even working on balloon payloads for other projects. Support is requested for one 40 hour-per-week undergraduate each summer.
  - There is partial summer salary support for Aguirre and Devlin. The JPL subcontract provides partial support to Bradford.
  - For calculation of overhead, Modified direct cost = total direct cost - equipment - tuition
- **Travel.** The travel budget for STARFIRE is dominated by the field travel for two one-month campaigns in Palestine or Ft. Sumner. We have been in the field several times with our instruments

and have experience conserving resources (such as renting houses instead of individual rooms in hotels). In addition, there is the necessary travel back-and-forth between JPL and Penn for training and assistance with testing and integration (cross-pollination of the postdocs and graduate students) and also during years 4 and 5 for collaborative work on data analysis. We have estimated \$60,000 for domestic travel over the five years. In addition, \$5,000 in foreign travel is requested for travel to conferences to present results.

- **Lab Supplies.** This covers miscellaneous hardware and tools required for construction and testing, as well as flight operations. A total of \$60,000 over 5 years is requested, with higher amounts in years 3 and 4 for contingency in preparing for the first flight.
- **Cryogens.** These are for flight operations as well as running multiple laboratory tests. As much as possible, we will use an existing closed-cycle cryogenic system (see Facilities and Resources) to conduct cold tests and thus conserve cryogens. Estimated costs are based on an inflation-adjusted average of \$10 per liquid liter, and a consumption rate of the cryostat of 100 liters on cooldown and 10 liters per day thereafter. Thus, a two-week cooldown costs approximately \$1500, allowing for boiloff and transfer losses. We request \$12,000 per year (8 two-week cooldowns) for each year we have the cryostat (years 2 - 5)
- **Publication.** We expect to have a significant number of papers from our flight within a short period after data collection, and so we have included the cost of publications years 4 and 5 of the grant. A total of \$10,000 is requested, amounting to about four large publications.
- **Subcontracts** There is a subcontract to JPL, with budget attached separately. The JPL award will be made directly from NASA.
- **Equipment**

- **Cryostat.** We have based the cost on the Z-Spec dewar, which has a 48-hour hold time and ample cryogenic volume for the spectrometer optics. It includes the cost for the He3/He4 fridges and magnetic shielding. The housekeeping thermometry and optics are specified separately. Total cost is estimated at \$50,000.
- **Cryostat Electronics.** This includes cryogenic housekeeping thermometers and cables, and their readout electronics, based on the BLAST design and experience. No significant change is anticipated over the BLAST budget, so we have simply reproduced the request, \$60,000.
- **Adiabatic Demagnetization Refrigerator (ADR).** This provides the final stage of cooling of the detectors to 160 mK. The cost of \$60,000 is based on a commercially available system quoted by High Precision Devices, Inc (HPD) in Boulder, Colorado.
- **Pointing Electronics.** This includes all of the electronics to run the gondola. There are two computers, power distribution, pointing sensors and star cameras, and interface boards to the motors and pointing sensors. Again, this is based on the BLAST design, which will be replicated, at a cost of \$60,000.
- **Gondola.** We will re-use the BLAST 2010 gondola. The cost here (\$10,000) is for a new inner frame to support the larger, heavier off-axis mirror.
- **Gondola Motors.** The BLAST drive motors will need to be redesigned for the larger mass and moment of the STARFIRE primary mirror and cryostat, at an estimated cost of \$30,000.
- **Primary Mirror.** The primary mirror cost is based on a detailed estimate by Magna Machining using a SolidWorks model of our current design, and including tolerance requirements. The \$400,000 cost includes material, lightweighting machining, and surface cutting

and polishing of *two* 2.5-meter off-axis mirrors. Because the surface cutting is done on a vertical lathe, both mirrors can be cut simultaneously. The second mirror provides a spare without significantly increasing the cost.

- **Secondary Mirror.** This is for the secondary mirror and positioning system. This is a nearly exact clone of the BLAST design, and is costed accordingly. Costs include the machining of the mirror surface and lightweighting for the mirror, as well as the focus-adjust mount for the mirror, its linear actuators, and the electronics, estimated at \$50,000.
- **Cold Optics.** This is for the machining of the cold image slicing and relay optics, the diffraction gratings, the blocking filters, their support structures, and the mechanism for moving the grating. The optical design calls for two spectrometer modules, each fed by an image slicer. Each spectrometer module has two mirrors (4 total), all of which are powered. The surface accuracy of these mirrors can be achieved with a machining process, and the largest of them is  $\sim$ 20 cm. In addition, there are two blazed diffraction gratings. Based on experience with the ZEUS spectrometer, the gratings are available commercially at an expected cost per grating of approximately \$15,000, and for mirrors of similar size and accuracy, the typical cost is \$3,000 - \$5,000, depending on size, averaging about \$4,000. Each module also requires positioning and alignment structures. We estimate a combined cost of \$62,000 for both spectrometer modules. The image slicing optics are much smaller, but require high alignment precision. Combined with the necessary mounting hardware, we estimate \$25,000 for each slicer, for a total of \$112,000.
- **Lenslet Arrays** These are the silicon lenses for focusing light on the KIDs. Four are required, one for each array, from VeldLaser at \$2000 each (as scaled from our prototype), for a total of \$8,000.
- **Detector Readout Electronics** This is the frequency multiplexed readout for the kinetic inductance detectors (KIDs). The cost includes \$14,000 for 4 SiGe amplifiers from Sandy Weinreb at Caltech (\$3.5k each), \$10,000 for 4 sets of cryogenic coaxial cable (\$2.2k for 2 NbTi runs (for  $T < 4$  K) and \$300 for 2 stainless runs), \$22,000 for the ROACH electronics (two systems, each handling 2 readout chains). Each ROACH system consists of: ROACH-1 board (\$2500), XC5VSX95T FPGA (\$2250), iStar chassis (\$515), ADC / DAC combo cards from Rick Raffanti (\$2650), and a readout computer (\$3000) which also handles data storage. The total cost of the readout system is \$48,000.

## Summary of Personnel Commitments and Costs

Individual		FY12	FY13	FY14	FY15	FY16
J. Aguirre	Penn	0.35 / 0.08	0.35 / 0.08	0.35 / 0.08	0.35 / 0.08	0.35 / 0.08
M. Devlin	Penn	0.20 / 0.04	0.20 / 0.04	0.20 / 0.04	0.20 / 0.04	0.20 / 0.04
J. Klein	Penn	0.00 / 0.00	0.00 / 0.00	0.17 / 0.17	0.17 / 0.17	0.17 / 0.17
S. Dicker	Penn	0.33 / 0.33	0.33 / 0.33	0.33 / 0.00	0.00 / 0.00	0.00 / 0.00
Postdoc 1	Penn	1.00 / 1.00	1.00 / 1.00	1.00 / 1.00	0.00 / 0.00	0.00 / 0.00
Postdoc 2	Penn	0.00 / 0.00	0.00 / 0.00	1.00 / 1.00	1.00 / 1.00	1.00 / 1.00
Graduate Student 1	Penn	1.00 / 1.00	1.00 / 1.00	1.00 / 1.00	1.00 / 1.00	1.00 / 1.00
Graduate Student 2	Penn	1.00 / 1.00	1.00 / 1.00	1.00 / 1.00	1.00 / 1.00	1.00 / 1.00
<b>TOTAL</b>		<b>3.88 / 3.45</b>	<b>3.88 / 3.45</b>	<b>5.05 / 4.62</b>	<b>3.72 / 3.29</b>	<b>3.72 / 3.29</b>

This table summarizes the time commitments of personnel contributing to this project in fractions of a year, *exclusive of JPL*. For this, see their itemized budget. The first number in each fiscal year column indicates the time commitment available for this work. The second gives the amount supported by this proposal. These numbers refer to a schedule that includes teaching and administrative duties.

## Facilities, Equipment and Other Resources

### Penn

*Existing Designs, Instrumentation and Equipment.* STARFIRE will rely heavily on existing designs and instrumentation from BLAST, ACT, and other projects. Whenever possible we will share equipment with BLAST. This includes systems such as the star cameras and other pointing sensors. We also have complete laboratory and field supplies that will be used for STARFIRE.

*Laboratory.* The University of Pennsylvania is equipped with a high bay facility in which BLAST-pol is currently undergoing integration. This facility will be sufficient for the integration of the STARFIRE gondola. Between Profs. Aguirre and Devlin there is approximately 1,800 ft<sup>2</sup> of space allocated for this work and can use 600 ft<sup>2</sup> more if necessary. All of the rooms are plumbed for a vacuum system and compressor. The ceilings have hard attachment points to mount 2-ton hoists. One of the rooms is accessible by fork-lift from the loading dock to move large pieces of equipment.

*Shops.* The physics department machine shop at Penn will be used to manufacture most of the parts. A CNC milling machine and lathe are available with a skilled machinist. The electronics lab at Penn is extremely knowledgeable and their services can be made available as needed.

*Computation and Data Storage.* Aguirre maintains the central computer cluster for PAPER data analysis and archival at Penn. This consists of 16 high-speed compute nodes as well as > 100 TB of storage. This facility will be upgraded over the next two years as part of NSF grant AST 1125558 “Collaborative Research: Precision Array for Probing the Epoch of Reionization (PAPER)”, at no cost to this grant. The computational needs of STARFIRE are minor compared to the resources available from this shared resource.

The following equipment at Penn will be available for use on this project:

- *Dedicated test cryostat* A cryostat with pulse-tube cooler, <sup>4</sup>He and <sup>3</sup>He sorption fridges, and instrumentation will be available for testing detectors and other cryogenic tests to avoid the unnecessary use of liquid cryogens in the flight cryostat.
- *Cryogenic equipment.* Considerable infrastructure for supporting cryogenic measurements exists and are ready to be dedicated to this project.
- *Infrared Fourier Transform Spectrometer.* This was built at Penn by undergraduates and graduate students. It operates from 80 GHz to 1.2 THz and will be used to characterize the STARFIRE bandpass response.
- *Standard laboratory test equipment*

## Caltech

We have access to a 600-square-foot laboratory space which is earmarked for this work. We have a dedicated cryostat fitted with coaxial leads and cooled to 300 mK with a combination of a 4-K Cryomech pulse tube refrigerator and a Chase  $^3\text{He}$  cooler. For initial measurements as our new readout is under development, we also have access to HEMT amplifiers (LNAs), a vector network analyzer (VNA), a 0–40 GHz frequency synthesizer, preamplifiers, IQ demodulators, digitizers and a data acquisition computer. These components allow the readout of a single channel using a standard homodyne detection technique.

For spectral profile measurement, we have both a long-throw ( $\delta\nu=300$  MHz) Fourier-transform spectrometer as well as tunable local-oscillator sources for all frequencies throughout our range.

Finally, we have a millimeter / submillimeter wave beam mapper formed from a chopped thermal source on a 2-D raster stage.

**Superconducting Device Fabrication at the Jet Propulsion Laboratory Microdevices Laboratory (MDL).** Dr H.G. ‘Rick’ LeDuc and his group at JPL maintains several sputter systems for the sputtering of high-quality superconducting films including Nb, Mo, Au, Ti, and Al and SiO<sub>2</sub> films. There are Unaxis Shutteline chlorine and fluorine inductively-coupled plasma (ICP) etchers in MDL for etching metal and dielectric films.

Key lithographic tools within the Microdevices Laboratory (MDL) include a Canon FPA300-EX3 projection stepper and a JEOL JBX-9300 FS electron beam writer. The stepper has a 0.6 numerical aperture and a KrF excimer laser light source (248nm) giving a resolution of 0.25  $\mu\text{m}$  and a high throughput rate. The electron beam writer has a field emission source and a 100kV accelerating potential producing a nominal 4nm electron beam diameter and nominal 20nm lines. These tools can be operated in a complementary mode in which the highest resolution patterns are written by the e-beam tool and matched with lower resolution patterns exposed by the stepper to maximize wafer throughput.

**Computing.** We have access to Caltech Astronomy Data Processing Facility, which hosts and maintains licenses for various electromagnetic simulation and data analysis software such as L-Edit, HFSS, Sonnet, ADS, IDL, and Matlab. We have included the cost for accounts and software licensing in our budget.